LITHOS 436–437 (2023) 106946

Contents lists available at ScienceDirect

LITHOS

journal homepage: www.elsevier.com/locate/lithos

Carboniferous mafic-ultramafic intrusions in the Eastern Pontides (Pulur Complex): Implications for the source of coeval voluminous granites

Gültekin Topuz [a,*], Rainer Altherr [b], Osman Candan [c], Jia-Min Wang [d], Aral I. Okay [a], Fu-Yuan Wu [d], Ali Ergen [e], Thomas Zack [f], Wolfgang Siebel [g], Cosmas K. Shangh [h], Winfried H. Schwarz [b], Hans-Peter Meyer [b], Muharrem Satır [h]

[a] İstanbul Teknik Üniversitesi, Avrasya Yer Bilimleri Enstitüsü, TR-34469 Ayazağa, İstanbul, Turkey
[b] Institut für Geowissenschaften, Universität Heidelberg, Im Neuenheimer Feld 234-236, 69120 Heidelberg, Germany
[c] Dokuz Eylül Üniversitesi, Jeoloji Mühendisliği Bölümü, Tınaztepe Yerleşkesi, Buca, İzmir, Turkey
[d] State Key Laboratory of Lithospheric Evolution, Institute of Geology and Geophysics, Chinese Academy of Sciences, Beijing 100029, China
[e] Maden Tetkik ve Arama Genel Müdürlüğü, Jeoloji Etütleri Dairesi, 06800, Çankaya, Ankara, Turkey
[f] Department of Earth Sciences, University of Gothenburg, 40530 Gothenburg, Sweden
[g] Institut für Geo- und Umweltnaturwissenschaften, Universität Freiburg im Breisgau, Albertstr. 23b, 79104 Freiburg, Germany
[h] Institut für Geowissenschaften (Geochemie), Universität Tübingen, Wilhelmstrasse 56, 72074 Tübingen, Germany

ARTICLE INFO

Keywords:
Mafic-ultramafic intrusion
Cumulate rock
High-K calc-alkaline granite
Isotopic dating
Variscan orogeny, Pulur
Sakarya Zone, Turkey
High-volume magmatism

ABSTRACT

This study deals with the age and petrogenesis of mafic-ultramafic intrusions ranging in size from a few meters to 10 km within the Early Carboniferous high-grade gneisses of the Pulur Complex in the Eastern Pontides. The intrusions comprise dunite, wehrlite, gabbronorite, leucogabbro, anorthosite and ilmenite-bearing gabbronorite of cumulus origin, and are crosscut by dikes of ilmenite-bearing gabbronorite, leucogranite and microdiorite. U–Pb dating on zircons from gabbronorite, anorthosite and leucogranite yielded igneous crystallization ages of 322–326 Ma, indicating that the intrusions were emplaced ca. 5–7 Ma after the peak of high-grade metamorphism, and form part of the Late Carboniferous high-volume magmatism in the region. In most cumulate rocks, Cr–Al spinel, olivine and plagioclase were early crystallizing phases, followed by orthopyroxene, clinopyroxene and hornblende. Whole rock geochemical data suggest that wehrlite, gabbronorite, leucogabbro and anorthosite stem from a common magma, and ilmenite-bearing gabbronorite and dikes of leucogranite and microdiorite from different magmas. Application of mineral/melt partition coefficients to trace element compositions of clinopyroxene and hornblende in cumulate rocks suggests that the main cumulate body was derived from middle- to high-K calc-alkaline basic melts, and relatively late ilmenite-bearing gabbronorites from hypersthene-normative Ca-rich melts. All the rock types display radiogenic Sr and Pb isotopic signatures, and unradiogenic Nd isotopic ratios, which are indistinguishable from those of the coeval voluminous high-K calc-alkaline I-type granites in the region; the isotopic ratios are probably related to the metasomatism of the lithospheric mantle by sediment-derived melts. We suggest that the parental melts of the mafic-ultramafic intrusions and those of the high-K calc-alkaline granites were genetically related, and melts of the high-K calc-alkaline granites were probably derived from the melting of newly underplated calc-alkaline basic material at lower crustal depths, that were compositionally comparable to the parental magmas of the mafic-ultramafic intrusions.

1. Introduction

A major part of the pre-Triassic basement of the Sakarya Zone (northern Turkey), about 70% of the basement exposures, consists of Carboniferous to Early Permian granitic rocks (Fig. 1) (Dokuz, 2011; Kaygusuz et al., 2012, 2016; Nzegge et al., 2006; Topuz et al., 2010;

* Corresponding author.
E-mail addresses: topuzg@itu.edu.tr (G. Topuz), rainer.altherr@geow.uni-heidelberg.de (R. Altherr), osman.candan@deu.edu.tr (O. Candan), wangjiamin@mail.iggcas.ac.cn (J.-M. Wang), okay@itu.edu.tr (A.I. Okay), wufuyuan@mail.iggcas.ac.cn (F.-Y. Wu), ali.ergen@mta.gov.tr (A. Ergen), thomas.zack@gu.se (T. Zack), wolfgang.siebel@uni-tuebingen.de (W. Siebel), winfried.schwarz@geow.uni-heidelberg.de (W.H. Schwarz), hans-peter.meyer@geow.uni-heidelberg.de (H.-P. Meyer), satir@uni-tuebingen.de (M. Satır).

https://doi.org/10.1016/j.lithos.2022.106946
Received 6 February 2022; Received in revised form 12 November 2022; Accepted 12 November 2022
Available online 18 November 2022
0024-4937/© 2022 Elsevier B.V. All rights reserved.

Ustaömer et al., 2012, 2013). The most significant pulse of granitic magmatism occurred during Late Carboniferous (326–315 Ma), as also shown by the pronounced peaks of the detrital zircon ages at 325–310 Ma in the Mesozoic sedimentary rocks (e.g., Akdoğan et al., 2017; Ustaömer et al., 2016). These granites are characterized by high-K calc-alkaline I-type affinity, and display "continental crust-like" isotopic signatures (Dokuz, 2011; Kaygusuz et al., 2012, 2016; Liu et al., 2018; Topuz et al., 2010). However, inherited zircons in the dated zircon populations are rare to non-existent. The origin of these voluminous granitic magmas is contentious. The proposed models include (i) melting of newly underplated mafic rocks by the injection of basaltic magmas from the upper mantle in a post-collisional setting (Topuz et al., 2010), (ii) mixing of felsic and basic magmas followed by crystal fractionation (Dokuz, 2011), and (iii) partial melting of early Paleozoic mafic to felsic lower crustal rocks, with minor contributions from the mantle (Kaygusuz et al., 2012, 2016). In marked contrast to the voluminous granitic rocks, coeval gabbroic rocks are not documented so far.

This study presents field geological, geochemical and geochronological data on the mafic-ultramafic intrusions in the Pulur complex (Eastern Pontides, NE Turkey). These so far undated intrusions were formerly interpreted as reversely zoned Alaskan-type mafic-ultramafic complexes which formed from high-Al hydrous basaltic magmas (Bektaş and Güven, 1996; Eyüboğlu et al., 2010). We demonstrate that the intrusions lack any obvious zonal structure, and comprise dunite, wehrlite, gabbronorite, anorthosite and ilmenite-bearing gabbronorite of cumulus origin. These rocks were derived through crystal fractionation and accumulation processes from middle- to high-K calc-alkaline basic magmas at mid-crustal depths at 326–322 Ma, i.e. concurrently with the most significant pulse of granitic magmatism after the thermal peak of the L to *MP-HT* metamorphism (331–328 Ma). We propose that the coeval voluminous high-K calc-alkaline I-type granitoids originated from the partial melting of underplated middle- to high-K calc-alkaline mafic rocks at the lower crustal depths.

2. Geological setting

Within the Tethyan realm, the Sakarya Zone is a Gondwanian continental block, which was accreted to Laurussia during the Early Carboniferous (Fig. 1 inset) (e.g. Akdoğan et al., 2021; Okay et al., 2006; Okay and Topuz, 2017; Topuz et al., 2010; Ustaömer et al., 2012, 2013). The southern boundary of the Sakarya Zone is delimited by the Izmir-Ankara-Erzincan suture which represents the trace of a long-lived Paleozoic to earliest Cenozoic oceanic domain (Okay et al., 2020; Topuz et al., 2013).

The basement rocks of the Sakarya Zone crop out in several inliers beneath the Lower Jurassic volcanic and sedimentary sequences, and can be divided basically into two different groups (i) a continental domain consisting of Early Carboniferous L to *MP-HT* metamorphic

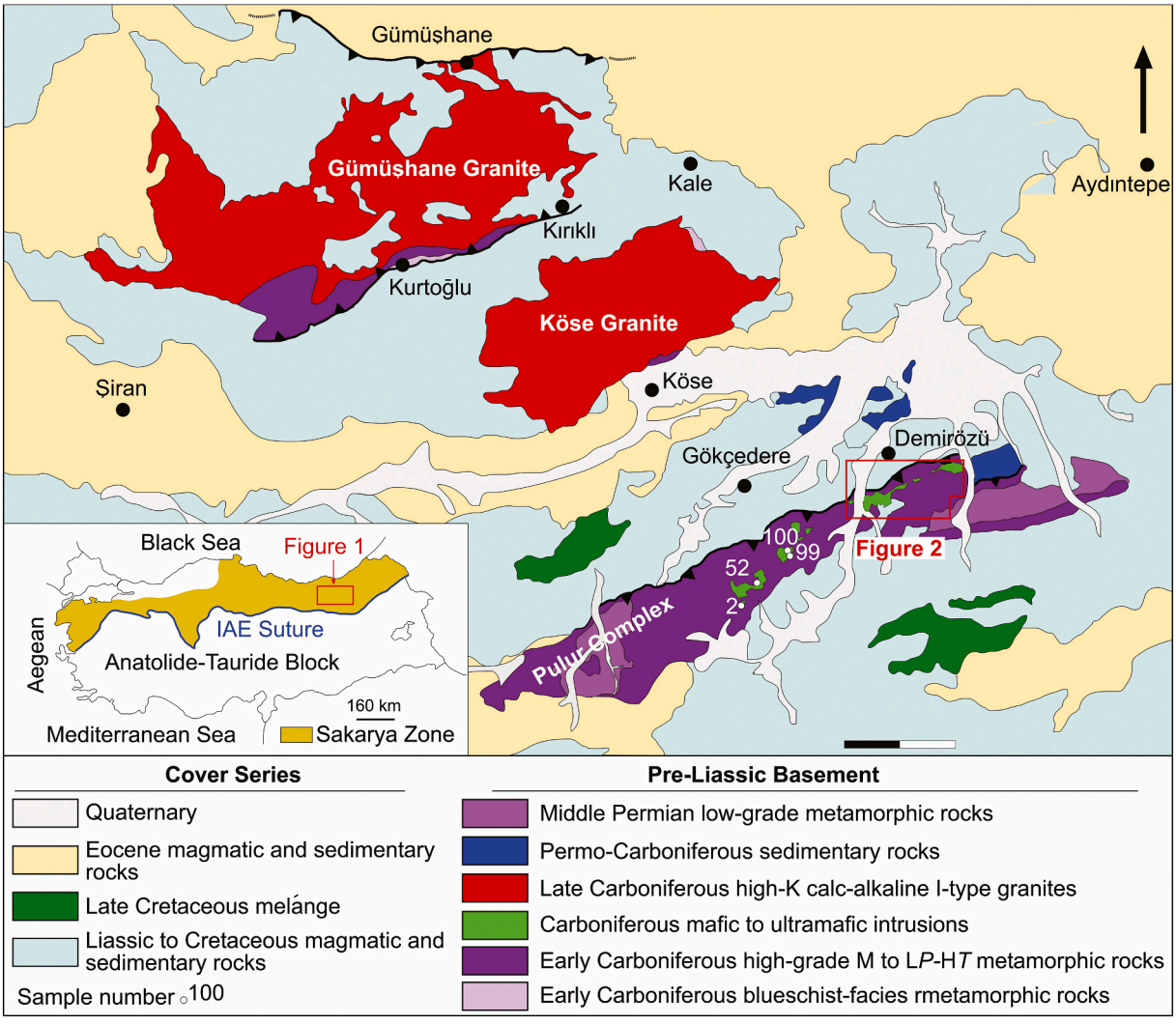

Fig. 1. Distribution of pre-Jurassic basement units in the southern part of the Eastern Pontides (modified after MTA, 2002). The inset shows the Sakarya Zone in Turkey.

units, Early Carboniferous to Permian intrusions and Upper Carboniferous-Lower Permian molassic sedimentary rocks (e.g. Dokuz, 2011; Dokuz et al., 2017; Karslı et al., 2016; Kaygusuz et al., 2012, 2016; Okay and Leven, 1996; Topuz et al., 2004a, 2007, 2010; Ustaömer et al., 2012, 2013), and (ii) Permo-Triassic low-*T* medium- to high-*P* metamorphic units, interpreted as accretion and subduction complexes (e.g. Okay and Göncüoğlu, 2004; Topuz et al., 2004b, 2014). Timing of the peak metamorphism in the Early Carboniferous L to M*P*-H*T* metamorphic units is constrained by U–Pb monazite ages at 332–328 Ma (e.g., Topuz et al., 2004a; Ustaömer et al., 2013). The Pulur mafic-ultramafic intrusions, the topic of this paper, occur in these Early Carboniferous L to M*P*-H*T* metamorphic rocks.

3. Pulur mafic-ultramafic intrusions

The Pulur Complex is a pre-Jurassic basement in the Eastern Pontides consisting of metamorphic and plutonic rocks overlain unconformably by Lower Jurassic volcaniclastic rocks (Fig. 1). In the Pulur complex, Early Carboniferous low to medium pressure-high temperature (L to M*P*-H*T*) metamorphic rocks are intruded by mafic-ultramafic intrusive bodies at several localities (e.g. Bektaş and Güven, 1996; Eyüboğlu et al., 2010). Single intrusive bodies vary in size from a few meters to about 10 km in the longest dimension (Fig. 2). Overall, the rocks are devoid of any pervasive ductile deformation, suggesting that the emplacement of the intrusive bodies postdates the development of foliation in the country rocks. The intrusive contacts with the surrounding metamorphic country rocks are sharp and steeply dipping. However, chilled margins around the intrusive bodies are not observed, and contact metamorphic effects are not apparent. The intrusions are made up of ultramafic to felsic cumulate rocks including dunite, plagioclase-amphibole wehrlite, melagabbronorite, leucogabbro, anorthosite and ilmenite-bearing gabbronorite, and are intruded by dikes/veins of gabbro pegmatite, ilmenite-bearing gabbronorite, leucogranite, and late microdiorite. The contact relationships among different rock types are best exposed along a road cut to the south of the Karayaşmak village (Fig. 2).

The Karayaşmak intrusion, the largest intrusive body in the Pulur Complex, is ca. 1.5 km across and 10 km long, and is mainly surrounded by high-grade metamorphic rocks. To the south, the intrusion is partly overlain by an undated limestone. The Lower Jurassic volcaniclastic rocks, starting with a basal conglomerate, lie over the intrusion and the metamorphic rocks, indicating a pre-Jurassic emplacement age. The metamorphic country rocks consist of garnet-cordierite-sillimanite migmatites, mesocratic gneisses and amphibolites (Topuz et al., 2004a; Topuz and Altherr, 2004). Peak metamorphic conditions occurred at 0.8–0.7 GPa and ≥ 820 °C, followed by near-isothermal decompression to ~0.5–0.4 GPa at 800–730 °C. U–Pb monazite, Sm–Nd garnet, Rb–Sr and Ar–Ar biotite and muscovite dating suggest that the country rocks attained peak conditions at 332–328 Ma and cooled below 300 °C at about 310 Ma. The garnet-cordierite-sillimanite migmatites occur along the whole length of the Pulur Complex and are not only confined to the domains close to the contacts of the mafic-ultramafic intrusions. There is no noticeable increase of metamorphic grade towards the intrusions and contact metamorphism is not obvious in the country rocks, apart from a small marble block/layer in contact with quartz diorite, ca. 5 m in diameter, transformed to a coarse-grained calcsilicate granofels with grossularite-andradite-rich garnet, vesuvianite, plagioclase, quartz and calcite.

The Karayaşmak intrusion is made up of dunite, plagioclase-amphibole wehrlite, gabbronorite, anorthosite, microgabbro, pegmatitic gabbro, leucogranite and microdiorite. No obvious zonal structure has been confirmed in contrast to the descriptions of Eyüboğlu et al. (2010). The dunite is minor and occurs at one location (sample 438A). The relatively more abundant plagioclase-amphibole wehrlite crops out at several isolated places, and shows a characteristic dark color (Fig. 3a). With increasing plagioclase content, it grades into melagabbronorite, and includes locally up to 50 cm-thick layers of gabbronorite. The gabbronorite, which grades into anorthosite, is the dominant rock type and its contact with the plagioclase-amphibole wehrlite is sharp (Fig. 3b). The gabbronorite is relatively fine-grained, and locally contains clasts of plagioclase-amphibole wehrlite (Fig. 3c). These clasts

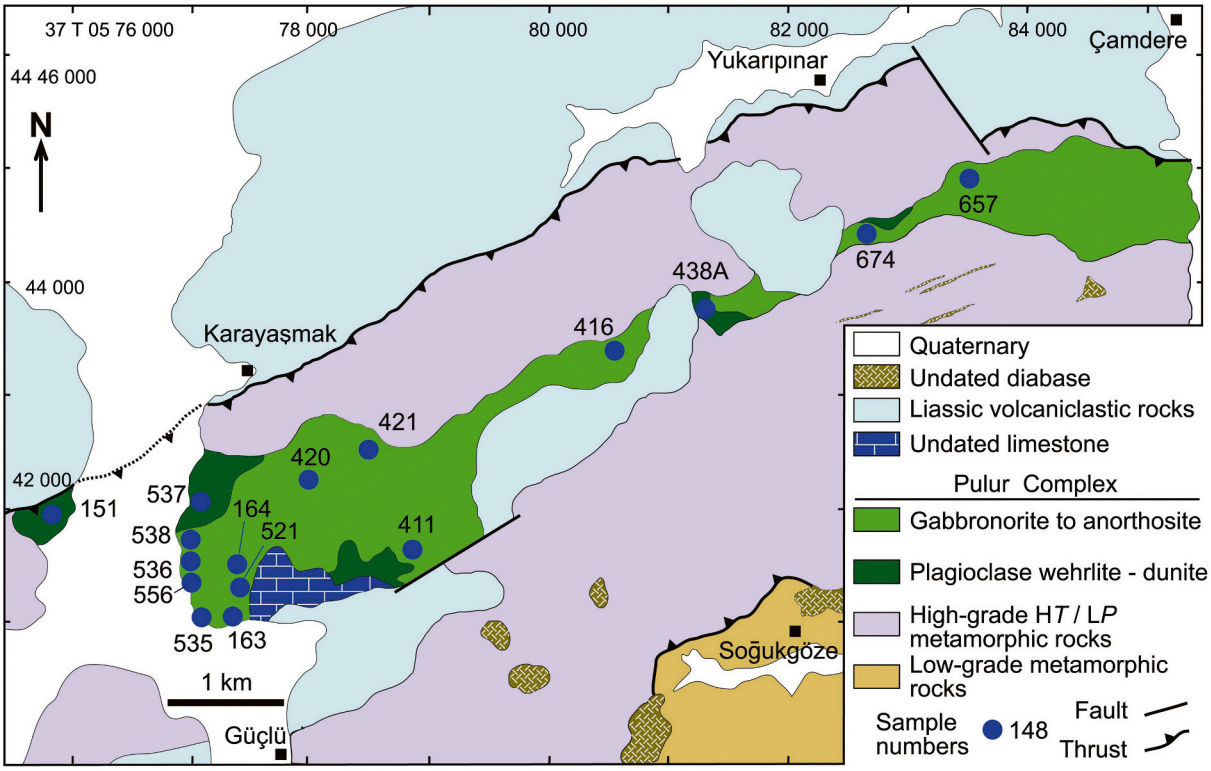

Fig. 2. Geological map of the Karayaşmak mafic-ultramafic intrusion in the Pulur Complex together with the sample locations.

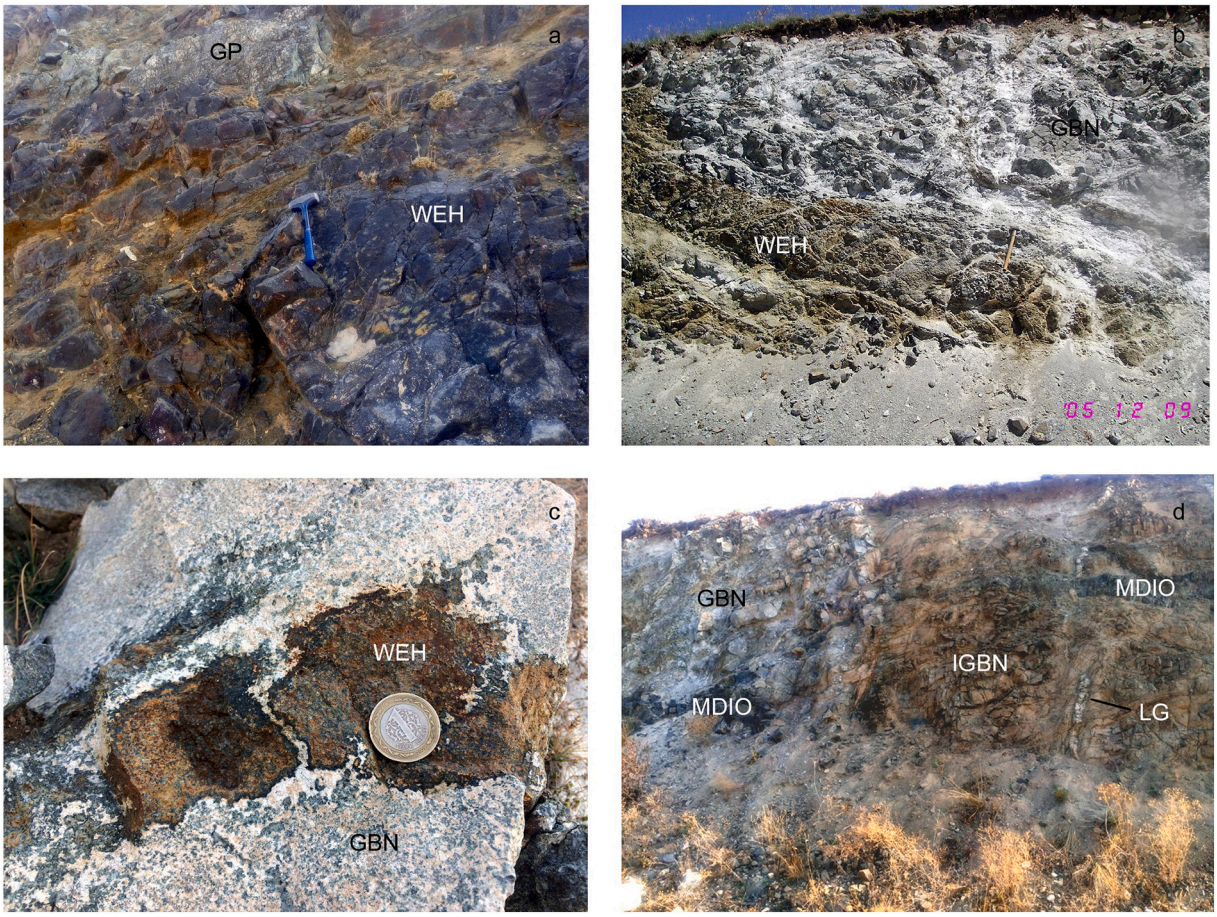

Fig. 3. Field photographs showing the relationships among the different rock types in the mafic-ultramafic intrusions. **a** Massive plagioclase-amphibole wehrlite (WEH) is crosscut by a vein of gabbroic pegmatite (GP). **b** Intrusive contact between gabbronorite (GBN) and wehrlite. **c** Fragments of wehrlite incorporated into gabbronorite. There is plagioclase- and hornblende-rich reaction rim between host gabbronorite and wehrlite. **d** Relatively fine-grained ilmenite-bearing gabbronorite (IGBN) is in intrusive contact with gabbronorite, and is crosscut by dykes of leucogranite (LG) and late microdiorite (MDIO).

range in size from 10 cm to one meter in diameter. Centimeter-thick reaction zones between the incorporated plagioclase-amphibole wehrlite and gabbronorite are present. This suggests that the plagioclase-amphibole wehrlite was semi-consolidated before the formation of the gabbronorite-anorthosite. Gabbronorite and anorthosite locally display modal layering defined by the alternation of plagioclase- and pyroxene-rich layers at cm- to dm-scale. There are 10 to 100 cm-thick veins of gabbroic pegmatite within the cumulate rocks (Fig. 3a). Contacts between gabbroic pegmatite and the host rock are sharp to diffuse. Ilmenite-bearing gabbronorite, mainly fine-grained, occurs as a late phase of the intrusion (Fig. 3d) or as up to 30 cm-thick dikes in all the cumulate rocks. These locally cross-cutting field relations rule out the formation of all the cumulate rocks in a large magma chamber by successive gravitational crystal settling and/or flotation and suggest that some cumulate rocks are probably related to later magmatic pulses. All these rock types are crosscut by leucogranite and microdiorite. Dikes of leucogranite range from 5 to 70 cm in thickness (Fig. 3d). Graphic texture, defined by the intergrowth of quartz and feldspar, is common in leucogranite. Dikes of microdiorite crosscut all the other dikes and rocks, and have thicknesses up to 10 m.

4. Analytical techniques

Analytical techniques are summarized below. Detailed descriptions can be found in the electronic appendix.

Major element compositions of mineral phases were determined at the Institute of Geosciences, Heidelberg University using a CAMECA SX51 electron microprobe equipped with five wavelength-dispersive spectrometers. Major element compositions of whole-rock samples were determined by XRF (modernized SRS 300 wavelength-dispersive spectrometer; Bruker AXS) at Heidelberg using Lithium borate fusion disks. Whole-rock trace elements were determined by laser ablation single-collector inductively coupled plasma mass spectrometry (LA-ICP-MS, Merchantek LUV213 coupled with ThermoFinnigan Element2) at the Institute of Geosciences, Frankfurt/M. University. Sr, Nd and Pb isotope analyses of whole-rock samples were performed at the Institute of Geosciences, Tübingen University. LA-ICP-MS U–Pb analyses and trace element compositions of zircon were obtained at the Institute of Geology and Geophysics, Chinese Academy of Sciences (IGGCAS), using an Agilent 7700 ICP-MS equipped with a pulsed 193-nm ArF Excimer laser system. Trace element compositions of olivine, orthopyroxene, clinopyroxene, hornblende and plagioclase were carried out by an Agilent 8800 ICP-MS equipped with a New Wave NWR213 laser ablation system at the Gothenburg University and Agilent 7700 ICP-MS equipped with a pulsed 193-nm ArF Excimer laser system at the Institute of Geology and Geophysics, Chinese Academy of Sciences (IGGCAS).

5. Petrography and mineral compositions

Based on textural and geochemical characteristics, the rock types were subdivided into cumulate and non-cumulate types. Cumulate rocks include dunite, plagioclase-amphibole wehrlite, gabbronorite, leucogabbro and anorthosite, and relatively younger ilmenite-bearing gabbronorite (type-I). Non-cumulate rocks occur mainly in form of late

dikes and are represented by type-II ilmenite-bearing gabbronorite, leucogranite and microdiorite. Mineral compositions were measured on twelve samples, and representative analyses are given in Tables S1 to S6. In cumulate rocks, igneous minerals are homogeneous and compositional variation at the thin-section scale is generally limited. In all cumulate and non-cumulate samples, X_{Mg} values [= Mg/(Mg + Fe^{2+}+ Fe^{3+})] are highest in the clinopyroxene followed by those of amphibole, orthopyroxene, olivine, and Cr–Al spinel (Table S7). The analyzed samples show variable degrees of hydrothermal alteration. Hydrothermal phases include actinolite, epidote, pumpellyite, prehnite, chlorite, muscovite, titanite, serpentine, talc, natrolite, alkali feldspar, magnetite, calcite, pyrite, chalcopyrite, and quartz.

Dunite samples are completely serpentinized and comprise serpentine and minor relic Cr–Al spinel and magnetite. Relic Cr–Al spinel is surrounded by magnetite. *Plagioclase-amphibole wehrlites* are characterized by abundant resorbed crystals of cumulus olivine (up to 5 mm in size; 65–80 vol%) accompanied by variable amounts of intercumulus clinopyroxene, amphibole and plagioclase (Fig. 4a). Plagioclase crystallization locally occurred later than clinopyroxene. Some wehrlite samples (e.g., 537B) also contain intercumulus orthopyroxene, suggesting transition to lherzolite. Cr–Al spinel occurs as inclusion in olivine. Amphibole may contain relicts of clinopyroxene, suggesting relatively late igneous growth. Accessory chloritized biotite replacing amphibole was observed in some samples. Clinopyroxene and amphibole may form oikocrysts. The amount of plagioclase is variable. Plagioclase-rich wehrlite layers grade into melagabbronorite (416A). In all wehrlite samples, olivine is heavily serpentinized and plagioclase is largely replaced by secondary phases such as prehnite, calcite,

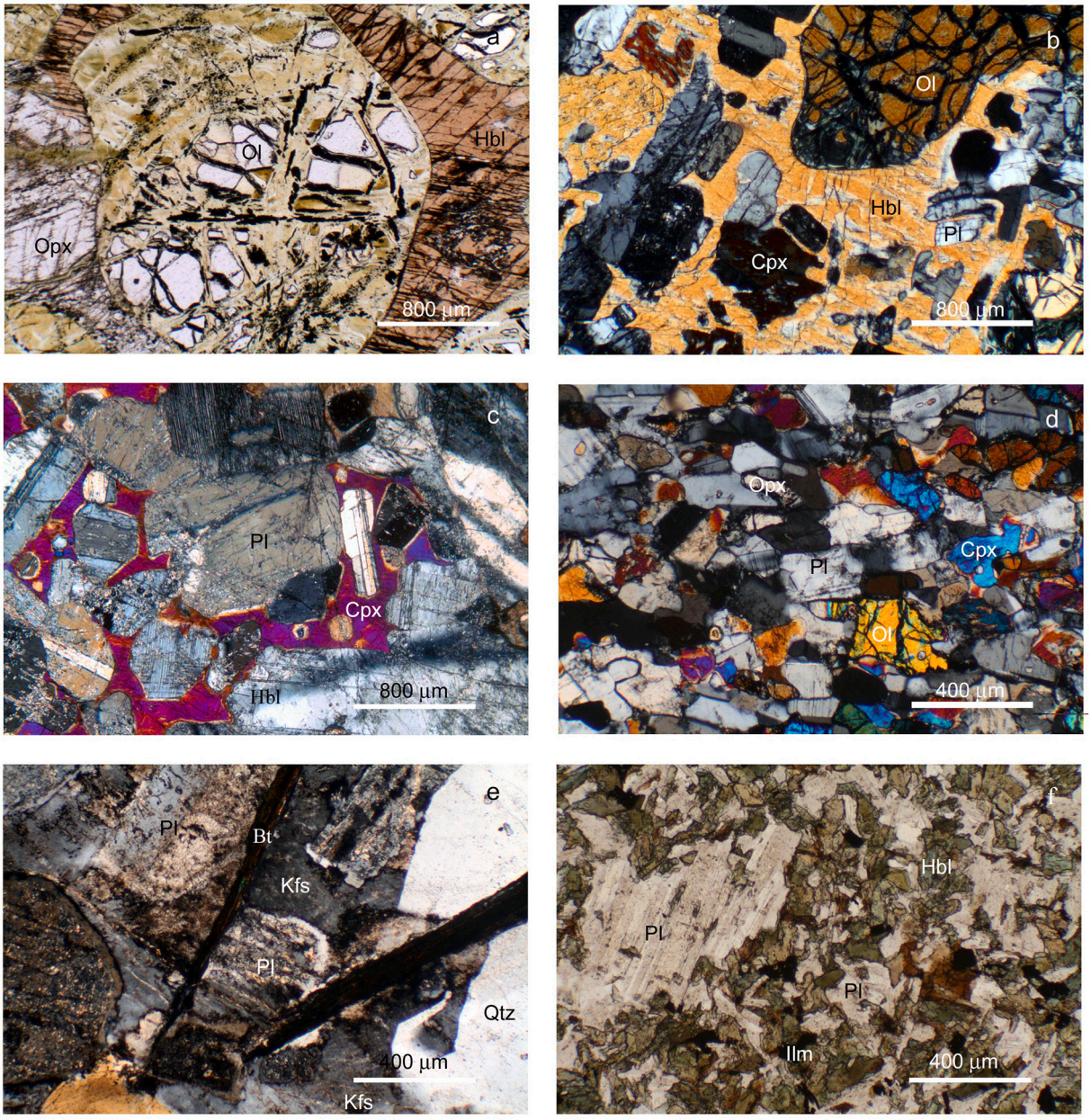

Fig. 4. Photomicrographs showing microtextural features of the different rock types in the mafic-ultramafic intrusions. **a** Partially serpentinized cumulus olivine (Ol) surrounded by intercumulus orthopyroxene (Opx) and hornblende (Hbl) in wehrlite (411D). **b** Intercumulus Hbl surrounds Ol, Pl and clinopyroxene (Cpx) in a gabbronorite (2C). Ol and Cpx display anhedral resorbed outlines. **c** An oikocryst-like Cpx includes Pl and Ol in anorthosite (420). A thin Hbl rims Cpx. **d** Fine-grained texture in ilmenite-bearing gabbronorite (164). **e** Pl, quartz (Qtz), chloritized biotite (Bt) and interstitial K-feldspar (Kfs) in leucogranite (537A). **f** Porphyric texture in microdiorite including Hbl, Pl, Bt and ilmenite (Ilm) (416D).

pumpellyite, clinozoisite and minor albite. Olivine in most wehrlites has a composition of $Fo_{85–80}$ (Table S1). Clinopyroxene is diopside with a high wollastonite component (Fig. 5a; Table S2). X_{Mg} values [= Mg/(Mg + Fe^{2+} + Fe^{3+})] range from 0.92 to 0.85. Ti, Al and Cr contents are relatively low (0.002–0.029, 0.014–0.137 and 0.007–0.028 cations per formula unit (cpfu), respectively) and increase with decreasing X_{Mg}, pointing to Ca- and Cr-Tschermark components. An increase of Al contents with decreasing X_{Mg} is commonly ascribed to the tschermak exchange [Al_2(Mg, Fe^{2+})$_{-1}$Si$_{-1}$] during cooling (Jagoutz et al., 2007; Rezeau et al., 2021). Na contents are generally low (< 0.021 cpfu). Most of the clinopyroxene analyses, when normalized to six oxygens and four cations, show a substantial Fe^{3+} content (0.030–0.056 cpfu). Orthopyroxene, when present, shows X_{Mg} values (0.83–0.84) that are significantly lower than those of clinopyroxene (0.87–0.90) (Fig. 5a-b; Table S3). Fe^{3+} contents are relatively high (0.030–0.065 cpfu). Ti and Al contents (0.009–0.013 and 0.055–0.066 cpfu, respectively) are low, and do not increase with decreasing Mg#. Cr–Al spinels are characterized by X_{Cr} [= Cr/(Cr + Al)] and X_{Fe2+} [= Fe^{2+}/(Mg + Fe^{2+})] of 0.52–0.58 and 0.65–0.75, respectively (Fig. 6; Table S4). X_{Fe3+} [= Fe^{3+}/(Cr + Al + Fe^{3+})] ratios are 0.05–0.07. Most Cr–Al spinel grains are homogenous, but some grains show slight zoning with rimward increases of Fe^{2+} and Al and decreases of Mg, Cr and Ti. Cr–Al spinel included in olivine has higher X_{Fe2+} than interstitial Cr–Al spinel grains or those included in orthopyroxene or clinopyroxene, while X_{Cr} values are roughly similar. This suggests redistribution of Fe–Mg between olivine and Cr–Al spinel in response to decreasing temperatures. Amphibole (Table S5) has relatively high X_{Mg} values (0.86–0.82), ^{IV}Al (1.51–1.76 cpfu) and A-site occupancy (0.55–0.68 cpfu), and is classified mainly as pargasite and magnesio-hornblende (Fig. 7).

Gabbronorites are medium to coarse-grained. Olivine and plagioclase were the first crystallizing phases (Fig. 4b). Olivine has subhedral to anhedral outlines. Plagioclase occurs either as small (< 150 μm) euhedral laths included in olivine, clinopyroxene and amphibole or as large (up to 3 mm) discrete crystals. This textural feature suggests that adcumulus growth of plagioclase continued during the crystallization of intercumulus phases. Orthopyroxene often appears in overgrowth relation with olivine. Overall, all the early crystallized phases (olivine, clinopyroxene, orthopyroxene and plagioclase) in large amphibole oikocrysts show resorbed outlines (Fig. 4b). Amphibole frequently forms oikocrysts including all other phases and locally replaces clinopyroxene. Cr–Al spinel occurs as tiny inclusions in all other phases. The gabbronorite differs from the ilmenite-bearing gabbronorite in the same intrusion by the presence of Cr–Al spinel and the absence of ilmenite. The composition of olivine ($Fo_{79–67}$, Table S1) is positively correlated with bulk rock Mg#. Forsterite-richer olivine occurs in samples with higher Mg#. Clinopyroxene has X_{Mg} values of 0.88–0.70, while the Ti and Al contents are relatively low and similar to those of clinopyroxene from the wehrlites (Fig. 5b; Table S2). No evidence for systematic core-to-rim zoning was found. Orthopyroxene has X_{Mg} values between 0.86 and 0.78 and relatively high Fe^{3+} contents (Fig. 5b; Table S3). Amphibole is characterized by X_{Mg} values of 0.80–0.70, ^{IV}Al contents of 1.77–1.56 pfu and A-site occupancies of 0.57 to 0.45 cpfu (pargasite to tschermakite) (Fig. 7; Table S5). Due to the small grain size, the composition of Cr–Al spinel could not be analyzed. Plagioclase has $An_{93–84}$ (Table S6).

Leucogabbros and anorthosites display a cumulate texture characterized by isolated olivine grains embedded in cumulus plagioclase (Fig. 4c). Intercumulus phases are oikocrystic clinopyroxene and amphibole. In addition, accessory amounts of intercumulus orthopyroxene may be present. Cr–Al spinel occurs as small inclusions in olivine and plagioclase. As leucogabbros and anorthosites form a continuous spectrum, the compositions of their minerals are described together. Olivine has a compositional range $Fo_{79–75}$ (Table S1). Clinopyroxene has X_{Mg} values of 0.89–0.80 and relatively high Ti and Al contents (Fig. 5a-b; Table S2). Cr–Al spinel is characterized by X_{Cr} and X_{Fe2+} ratios of 0.43–0.63 and 0.71–0.89 (Fig. 6; Table S4). These compositional features are typical of Cr–Al spinels from the magmatic arc-related intrusions, and different from abyssal and Alpine-type peridotites (e.g. Batanova et al., 2005; DeBari and Coleman, 1989; Dick and Bullen, 1984; Himmelberg and Loney, 1995; Jan and Windley, 1990; Spandler et al., 2003). Amphibole is also rich in Mg (X_{Mg} = 0.83–0.78), has ^{IV}Al contents of 1.38–1.60 pfu and A-site occupancies of 0.58–0.38 (Fig. 7; Table S5). These compositions correspond to the transition between magnesio-hornblende and pargasite. Plagioclase has $An_{93–86}$ (Table S6).

Ilmenite-bearing gabbronorites differ from the gabbronorites in the main cumulate body mainly by fine to medium-grained textures (Fig. 4d), the presence of ilmenite and the absence of Cr–Al spinel. Olivine forms early crystallized grains with local inclusions of clinopyroxene and plagioclase, suggesting that the crystallization of olivine continued throughout most of the crystallization history. Crystallization

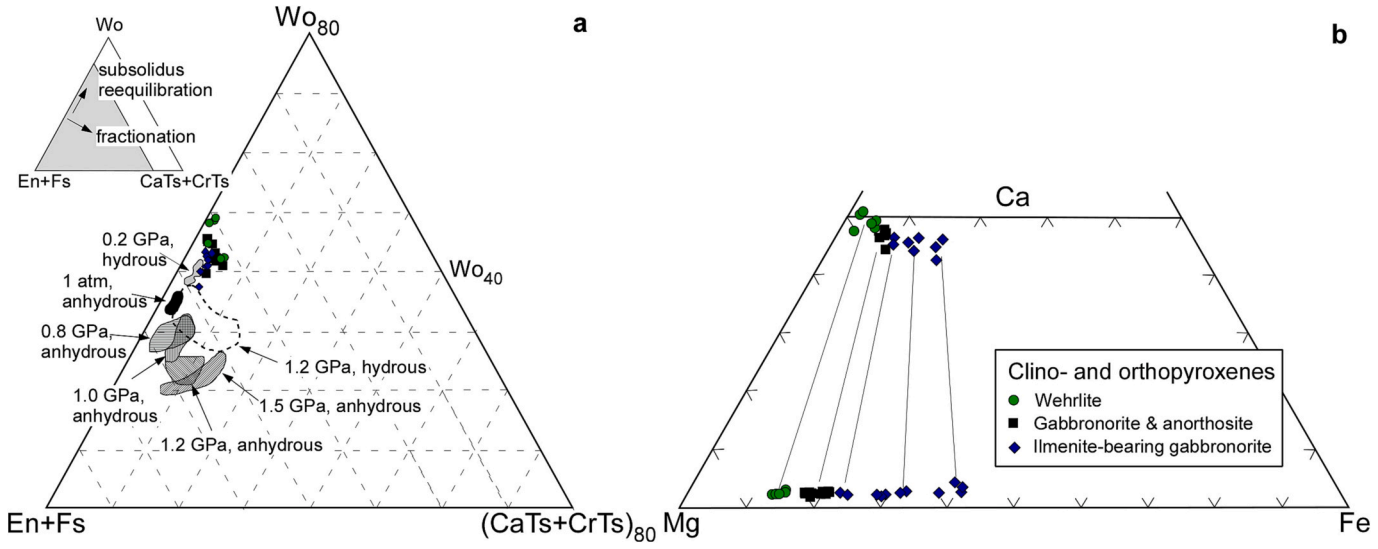

Fig. 5. **a** Clinopyroxene compositions plotted on the triangular diagram Wo ($CaSiO_3$) - En + Fs ($(Mg,Fe)SiO_3$) - CaTs+CrTs ($Ca(Al,Cr)SiAlO_6$) (modified after Gaetani et al., 1993). The dashed line stands for clinopyroxene compositions from the experimental work of Müntener et al. (2001) at 1.2 GPa. **b** Compositions of coexisting orthopyroxene and clinopyroxene in different rock types from the mafic-ultramafic cumulate intrusions in the Pulur Complex. Tie lines connect coexisting clino- and orthopyroxenes.

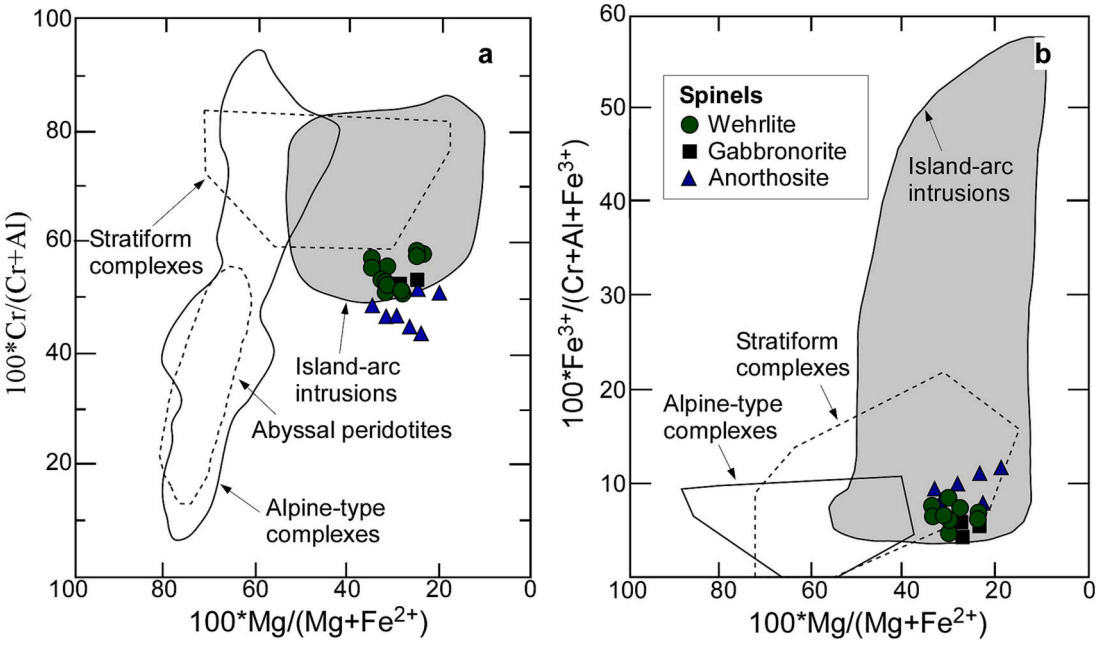

Fig. 6. **a** Compositions of Cr–Al spinel in the 100*Mg/(Mg + Fe^{2+}) versus 100*Cr/(Cr + Al) diagram. **b** in the 100*Mg/(Mg + Fe^{2+}) versus 100*Fe^{3+}/Cr + Al + Fe^{3+}) diagram. Data fields for island-arc intrusions, stratiform complexes, abyssal peridotites and Alpine-type complexes are from Burns (1985), Jan and Windley (1990) and Himmelberg and Loney (1995).

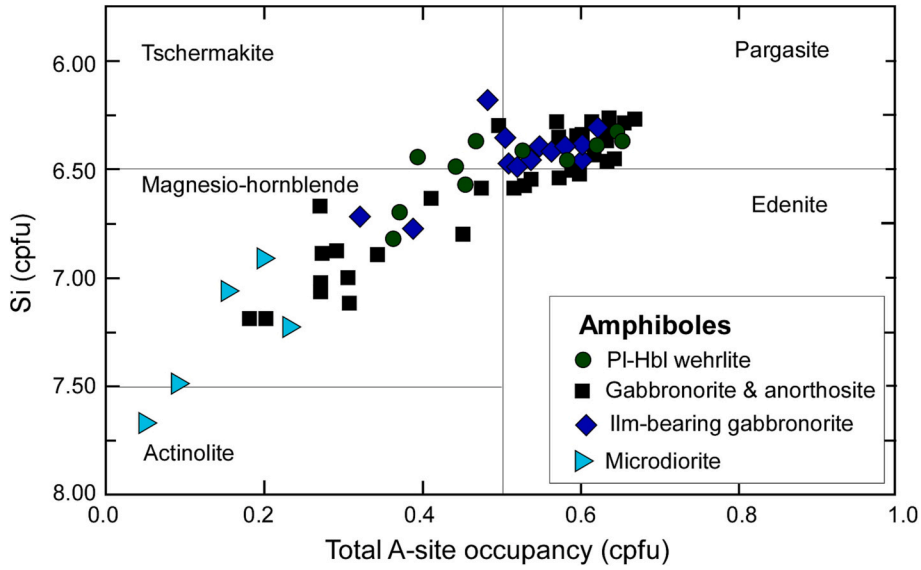

Fig. 7. A-site occupancy versus Si both in cations per formula unit (cpfu) of amphibole from the Pulur mafic-ultramafic intrusions. Nomenclature is after Hawthorne and Oberti (2007).

of clinopyroxene and plagioclase started before that of orthopyroxene. Clinopyroxene locally contains exsolution lamellae of orthopyroxene. Amphibole frequently fringes early-formed olivine or ilmenite and may also replace clinopyroxene. In clear distinction from the other cumulate rock types, the minerals show a large inter-sample compositional variation. Olivine has a wide-ranging composition ($Fo_{79–45}$) (Table S1). Clino- and orthopyroxenes have variable X_{Mg} values depending on the Mg# of the bulk rock (Fig. 5a-b; Tables S2 and S3). Ti and Al contents are low. Amphibole compositions are characterized by relatively high X_{Mg} values (depending on bulk-rock Mg#), ^{IV}Al contents of 1.49–1.78 and A-site occupancies of 0.37–0.66, thus classified as pargasite and magnesio-hornblende (Fig. 7; Table S5). Plagioclase grains are characterized by significant normal zoning and may contain relict An-rich cores resorbed by more Ab-rich outer zones. The overall (inter-sample) variation is relatively large ($An_{94–64}$) (Table S6). Ilmenite compositions correspond to $Ilm_{97–91}Gei_{00–04}Hem_{07–00}Pro_{01}$.

Leucogranitic dikes are medium-grained and consist of plagioclase, quartz, (perthitic) alkali feldspar and minor biotite (Fig. 4e). Accessory phases are apatite and zircon. Locally, plagioclase and quartz occur in micrographic intergrowths. Biotite forms bladed crystals, and is often transformed into chlorite and prehnite. Alkali feldspar is a late interstitial phase and may be transformed to albite. Plagioclase shows normal zoning ($An_{41–03}$) (Table S6). Compositions of primary alkali feldspar grains are $Or_{83–97}Ab_{17–03}An_{<01}$ (Table S7).

Microdioritic dikes are relatively coarse-grained and consist of amphibole (partly including relict clinopyroxene), plagioclase and

minor biotite (Fig. 4f). Amphibole is characterized by high contents of Si, low contents of Al, K and Na and by X_{Mg} values of about 0.44 and is classified as magnesio-hornblende and actinolite (Fig. 7; Table S5). Actinolite is probably related to alteration. Biotite is characterized by relatively low TiO_2 contents (3.30–2.18 wt%) and X_{Mg} values of 0.30–0.26. Plagioclase shows an extremely large compositional range ($An_{86–03}$), possibly partially related to late albitization (Table S6).

6. Whole-rock chemistry

Whole-rock analyses of 20 samples from the different rock types are given in Table S8. Loss on ignition values ranges from 1.20 to 10.20 wt %, reflecting the variably altered nature of the samples in line with the petrographic observations. The highest loss on ignition values is shown by plagioclase-amphibole wehrlites, and the lowest values by ilmenite-bearing gabbronorites. To enable sample comparison in terms of composition, the major element data are normalized on an anhydrous basis. It should be kept in mind that the bulk compositions in the cumulate rocks represent the total of the cumulus phases and the intercumulus phases grown from the trapped liquid, and thus do not correspond to the primary melt composition (e.g., Holness, 2021; Rollinson, 2008; Saccani and Tassinari, 2015).

Overall, rocks of *the cumulate suite (wehrlite, gabbronorite, leucogabbronorite and anorthosite except for type-1 ilmenite-bearing gabbronorite)* are characterized by low SiO_2 (40–48 wt%), highly variable Al_2O_3 (5–31 wt%) and CaO (3–15 wt%), and anomalously high Mg numbers (Mg# = 76–82). This wide-ranging compositional variation results from the accumulation of either olivine (high MgO) or plagioclase (high Al_2O_3).

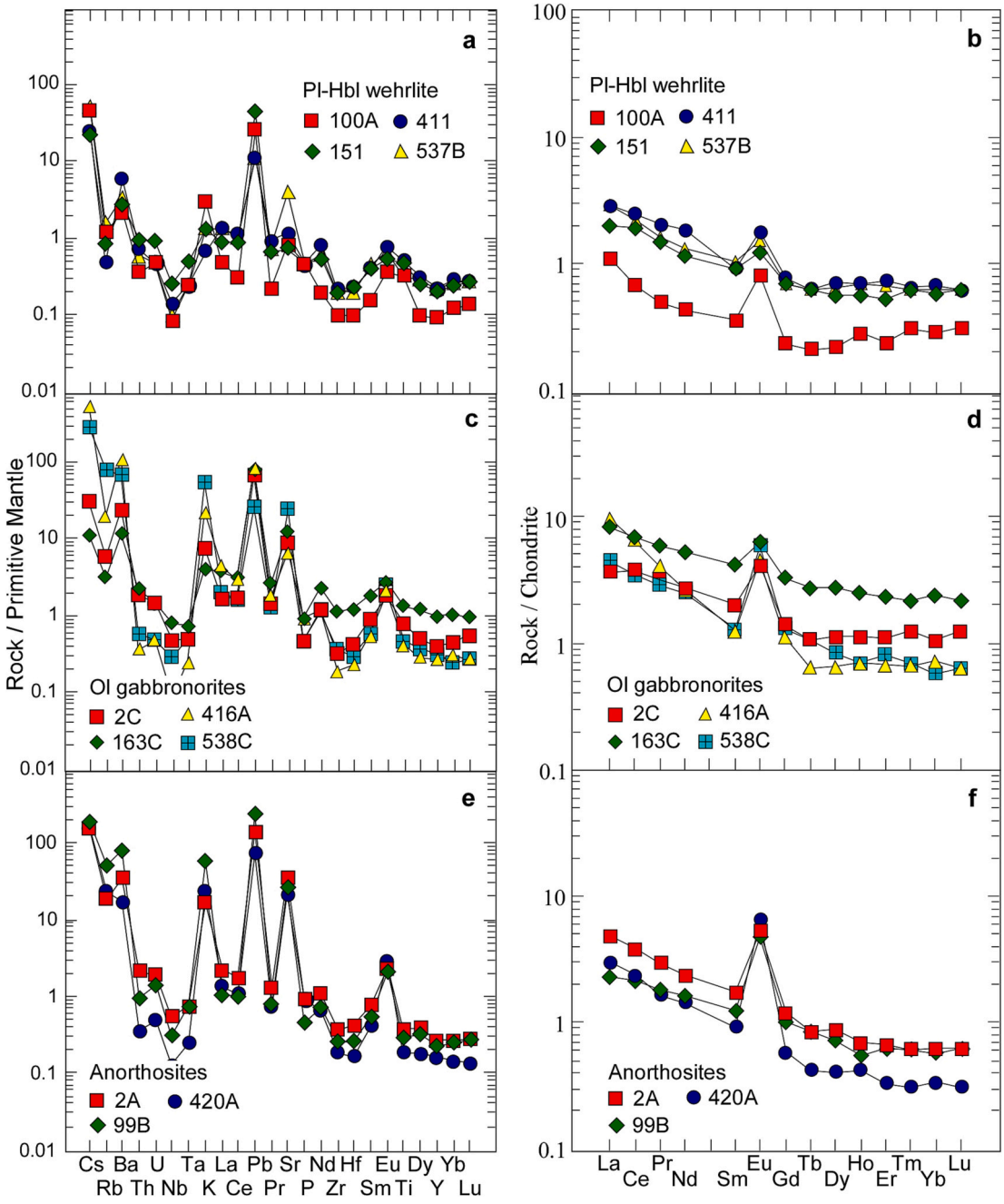

Fig. 8. Multi-element variation diagrams and rare earth element patterns for cumulate rock types from the Pulur Complex, normalized to primitive mantle after Sun and McDonough (1989) and chondrite after Boynton (1984), respectively.

The plagioclase-amphibole wehrlites have relatively constant Mg# (80–82), and gabbronorites and anorthosites slightly lower Mg# (76–80). In line with the high modal abundance of olivine, the plagioclase-amphibole wehrlites display relatively low CaO abundances (2–5 wt%) and high MgO abundances (28–30 wt%). On the other hand, the gabbronorites have variable CaO and MgO abundances, 5–15 and 7–22 wt%, respectively. The ilmenite-bearing gabbronorite (type-I) displays a narrow compositional range (SiO_2 = 45–48 wt%; Al_2O_3 = 20–21 wt%; CaO = 12–15 wt%; Mg# = 55–69). The samples of the non-cumulate rocks form discrete groups.

Despite variable alteration, all the samples display coherent geochemical characteristics (Figs. 8 and 9). Overall, the cumulate rocks are characterized by low concentrations of Zr, Y and REE. In the cumulate rocks, total concentrations of the rare earth elements are in the range of 1.62–16.32 ppm. The lowest REE concentrations are found in plagioclase-amphibole wehrlite (0.2 to 3 times chondritic), followed by anorthosite (0.2 to 5 times chondritic). The gabbronorites display the highest trace element and rare element concentrations (0.6 to 9 times chondritic). The REE patterns in all the cumulate rock types show a moderate enrichment of light REE over heavy REE ($(La/Yb)_{cn}$ = 4–13) with a significant positive Eu anomaly (Eu/Eu* [= $Eu_{cn}/(Sm_{cn}{*}Gd_{cn})^{0.5}$] = 2–9). On primitive mantle-normalized element concentration diagrams, they are characterized by (i) positive anomalies of Sr and Eu, and (ii) negative anomalies of Nb–Ta and Zr–Hf. Positive anomalies of Sr and Eu as well as moderate enrichment of light REE over heavy REE are caused by plagioclase accumulation and are most pronounced in anorthosites and leuco-gabbronorites.

Ilmenite-bearing gabbronorites have major and trace element compositions that indicate accumulation or fractionation of plagioclase (types I and II, respectively). Overall, the shape of the REE patterns of the ilmenite-bearing gabbronorites differs from that of the other cumulate rocks whereby the light REE are nearly flat (Fig. 8a-b). Based on whole-

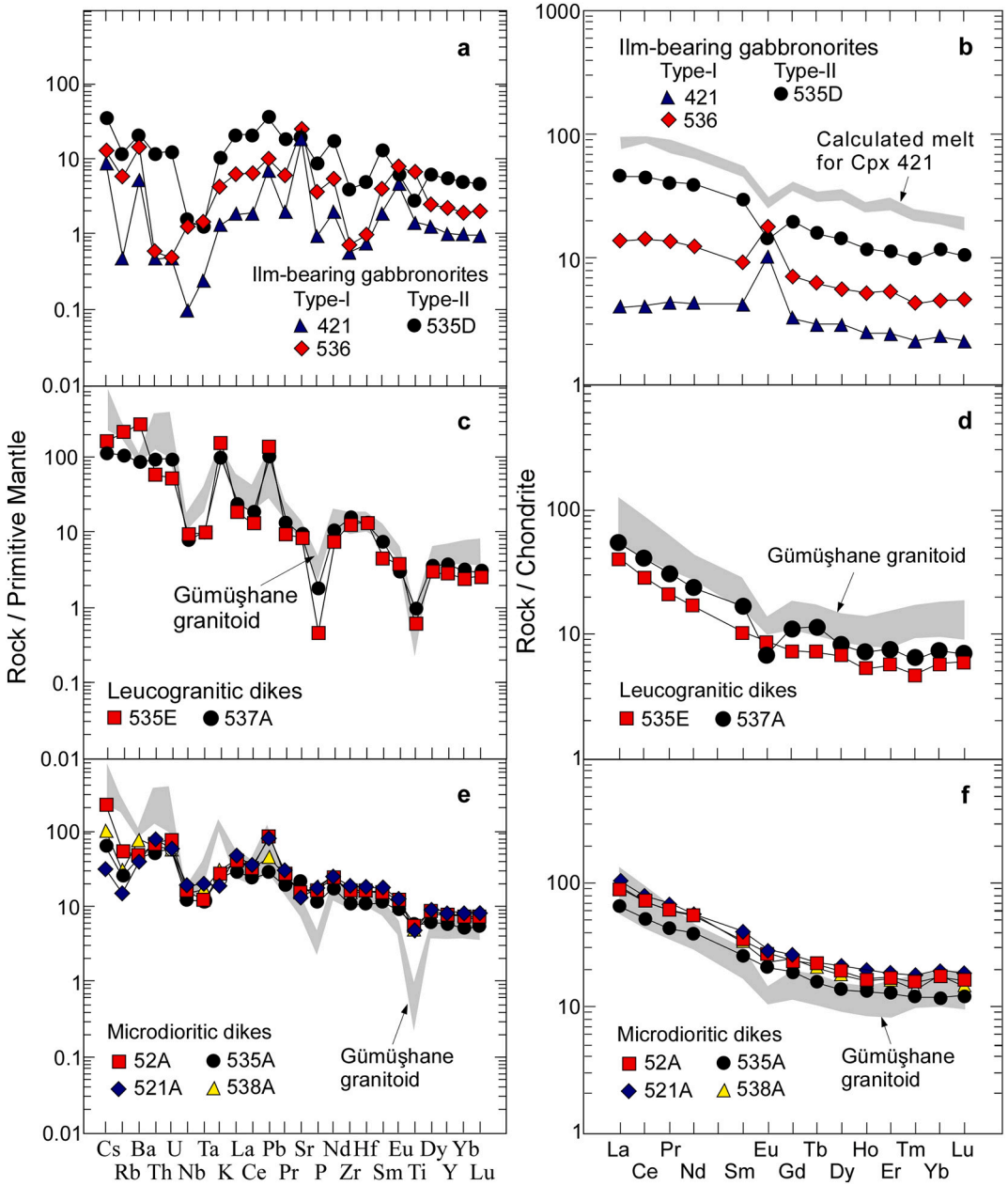

Fig. 9. Multi-element variation diagrams and rare earth element patterns of non-cumulate rock types from the Pulur Complex, normalized to primitive mantle after Sun and McDonough (1989) and chondrite after Boynton (1984), respectively.

rock chemistry (Table S8), two groups of samples can be distinguished: Type-I (samples 421 and 536) is characterized by low concentrations of REE and positive Eu and Sr anomalies, suggesting accumulation of plagioclase. Type II (sample 535D) has high concentrations of REE and negative Eu anomalies, suggesting considerable fractionation of plagioclase (Fig. 9a-b). In addition, type II has higher Zr, Hf and Pb than type I.

Leucogranitic dikes display a narrow range of SiO_2 (75–77 wt%; Table S8). Primitive mantle-normalized element concentration patterns are characterized by pronounced negative anomalies of Nb–Ta, P and Ti and positive anomalies of K and Pb (Fig. 9c). Chondrite-normalized REE patterns are concave-upward and show a relatively large enrichment of the light REE over the heavy REE ($(La/Yb)_{cn} = 7$) (Fig. 9d). Sample 537A has higher concentrations of MgO and $Fe_2O_3^{tot}$, and a higher Mg# value than sample 535E. Nevertheless, this sample shows a significant negative Eu anomaly (Eu/Eu* = 0.50) and relatively low Ba concentration, suggesting fractionation of plagioclase, which is in marked contrast to sample 535E which has no Eu anomaly and high Ba concentration.

Microdioritic dikes have SiO_2 concentrations between 56 and 61 wt% (Table S8). In a primitive mantle-normalized element concentration diagram, the rocks are characterized by negative Nb–Ta and Ti anomalies (Fig. 9e). The behavior of Pb is not systematic. The REE patterns are similar to those of the leucogranitic dikes, but with somewhat higher REE abundances (Fig. 9f). Sample 535A is the most primitive one (Mg# = 47) and has the highest CaO contents and lowest REE abundances. The other three samples have similar chemistry and significantly lower Mg# (~ 28), which is in line with their higher REE concentrations. Although all these rocks are significantly fractionated, they lack a negative Eu anomaly, suggesting that plagioclase played a minor role during magma fractionation in clear contrast to cumulate rocks. Most probably, fractional crystallization involved phases such as olivine, pyroxenes and hornblende.

Possibly due to the hydrothermal alteration, samples of the non-cumulate rocks do not show unambiguous discrimination in diagrams involving fluid-mobile elements (e.g., K_2O and Na_2O). On the Th–Co classification diagram after Hastie et al. (2007), designed for the hydrothermally altered igneous rocks, all the non-cumulate samples plot into the field of middle-K calc-alkaline series rocks (not shown). Their calc-alkaline nature is also substantiated by the slope and shape of the REE patterns (La/Yb > 6; Ross and Bédard, 2009).

7. Sr-Nd-Pb isotopic compositions

All the rocks are characterized by radiogenic Sr and Pb isotopic signatures, and unradiogenic Nd isotopic ratios: $^{87}Sr/^{86}Sr_{(i)}$ ranges from 0.70732 to 0.70851 and $\varepsilon_{Nd(i)}$ from −4.1 to −7.2 (both calculated back to 325 Ma) (Fig. 10a; Table S9). It is noteworthy that the plagioclase-amphibole wehrlites with the lowest Rb concentrations show enriched $^{87}Sr/^{86}Sr_{(i)}$ ratios, which are indistinguishable from those of gabbronorite and anorthosite. The Nd model ages, calculated according to the depleted mantle model of Liew and Hofmann (1988), range from 1.40 to 1.66 Ga. There are no noticeable isotopic differences between the cumulate and non-cumulate rock types. Notably, the Sr–Nd isotopic signatures of the mafic-ultramafic intrusions are indistinguishable from those of the voluminous Late Carboniferous granites (Fig. 10b) (Kaygusuz et al., 2012, 2016; Topuz et al., 2010). Only several samples from the Late Carboniferous granites with high Rb and low Sr concentrations show extremely low $^{87}Sr/^{86}Sr_{(i)}$ ratios, which were ascribed to hydrothermal alteration. In Pb–Pb isotope variation diagrams (Fig. 10c-d), the rocks plot above the Northern Hemisphere Reference Line (NHRL) of Hart (1984). $^{206}Pb/^{204}Pb(i)$ ratios vary from 18.10 to 18.57 and $^{207}Pb/^{204}Pb(i)$ and $^{208}Pb/^{204}Pb(i)$ ratios are relatively high (15.60–15.67 and 38.04–38.74, respectively). Samples cluster roughly in two groups whereby some samples display more radiogenic $^{208}Pb/^{204}Pb_{(i)}$ and $^{206}Pb/^{204}Pb_{(i)}$ ratios. There is, however, no apparent relationship between the rock types and the clusters.

8. Geochronology

To constrain the timing of the emplacement of the mafic-ultramafic intrusions, we have performed (i) single-grain evaporation dating on zircons from a leucogranite sample 556 intruding cumulate rocks, and (ii) LA-ICP-MS U–Pb dating on the zircons from three samples (657 gabbronorite, 674 anorthosite and 677 leucogranite). Sample locations are shown in Fig. 2. No dateable zircon could be extracted from the microdiorite dikes.

Zircon grains from leucogranite are euhedral and display oscillatory and sector zoning with very low luminescence (Fig. 11 inset). They are characterized by elevated U concentrations (1122–3894 ppm), relatively low Pb concentrations (94–195 ppm) and Th/U ratios of 0.22–0.39 (Tables S10 and S11). The low luminescence is probably caused by elevated U concentrations, as suggested by Poller et al.

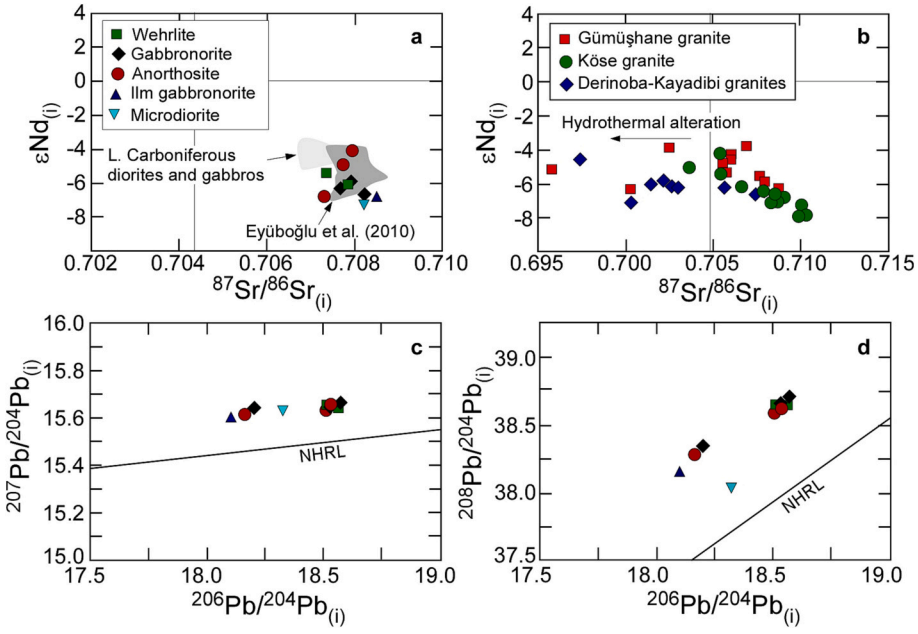

Fig. 10. **a** Variation of $^{87}Sr/^{86}Sr_{(i)}$ ratios versus $\varepsilon_{Nd(i)}$ values for the samples from the Pulur mafic-ultramafic intrusions. Also are shown isotopic compositions of latest Carboniferous gabbroic to dioritic rocks (Karslı et al., 2016), and of Pulur mafic-ultramafic rocks in Eyüboğlu et al. (2010), recalculated to 325 Ma. **b** $^{87}Sr/^{86}Sr_{(i)}$ ratios versus $\varepsilon_{Nd(i)}$ values of the Early to Late Carboniferous high-K calc-alkaline I-type granites. Data are from Topuz et al. (2010), Dokuz (2011), and Kaygusuz et al. (2012). **c-d** $^{207}Pb/^{204}Pb_{(i)}$ versus $^{206}Pb/^{204}Pb_{(i)}$ and $^{208}Pb/^{204}Pb_{(i)}$ versus $^{206}Pb/^{204}Pb_{(i)}$ ratios of the samples from the Pulur mafic-ultramafic cumulate rocks. NHRL = Northern Hemisphere Reference Line (Hart, 1984).

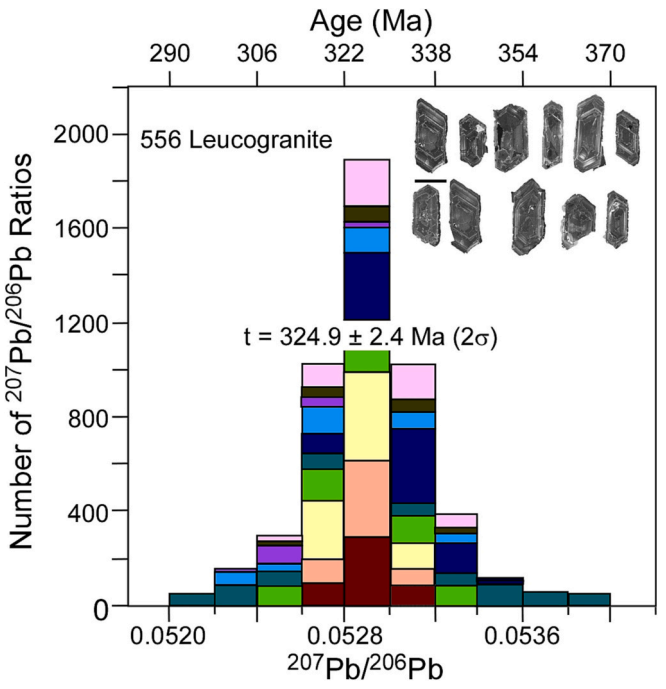

Fig. 11. Histogram showing the distribution of radiogenic $^{207}Pb/^{206}Pb$ ratios obtained from stepwise evaporation of four zircon grains from leucogranite sample 556. Inset shows CL images of the zircon grains.

(2001). On the other hand, zircon grains from gabbronorite and anorthosite samples are fractured and stubby crystals with oscillatory zoning (Fig. 12a and c, insets). The zircon grains from the anorthosite sample tend to have elevated U abundances (mostly >1000 ppm) which are comparable to those in the leucogranite, and significantly higher than those from the gabbronorite. Rare-earth element patterns of dated zircon grains are characterized by (i) enrichments of the HREEs with respect to the LREEs, (ii) pronounced negative Eu anomaly ($Eu/Eu^* = 0.07–0.58$), and (iii) pronounced positive Ce anomaly (Table S11). Thus, zircon growth in gabbronorite, anorthosite and leucogranite occurred from a melt in which plagioclase had already crystallized.

8.1. Single zircon evaporation dating

The Pb evaporation technique has been applied to ten zircon grains from leucogranite sample 556. The obtained $^{207}Pb/^{206}Pb$ ages range from 320.9 ± 2.4 to 330 ± 2.4 Ma (2σ) with a weighted mean of 324.9 ± 2.4 Ma (Fig. 11; Table S10). Only one zircon grain yielded a substantially lower $^{207}Pb/^{206}Pb$ age of 308.5 ± 2.6 Ma. Comparable $^{207}Pb/^{206}Pb$ ages for different temperature steps as well as similar ages for the different grains indicate the absence of a mixed-age population or older cores. The weighted mean $^{207}Pb/^{206}Pb$ age of 324.9 ± 2.4 Ma (2σ) is interpreted as the igneous crystallization age of the leucogranite dike.

8.2. LA-ICP-MS U–Pb zircon dating

LA-ICP-MS U–Pb dating have been applied on zircons from three samples (657: gabbronorite, 674 anorthosite and 677 leucogranite). From each sample, 30 grains were analyzed (Fig. 12a-b; Table S11). In all three samples, most concordant analyses cluster between 310 and 340 Ma. Several analyses, either concordant or discordant, yielded variably younger $^{206}Pb/^{238}U$ ages, caused probably by Pb loss. These analyses define a linear array, especially in sample 674. Besides, sample 657 contains two substantially older grains with $^{206}Pb/^{238}U$ ages of 391 ± 8 and 786 ± 22 Ma (2σ). Totally 21 grains from sample 657 and 17 grains from sample 674 yielded concordia ages of 322.6 ± 2.5 Ma (2σ, MSWD = 0.23) and 325.9 ± 1.4 Ma (2σ, MSWD = 2.8) (Fig. 12c-d). A concordia age cannot be calculated for the zircon grains from leucogranite 677, as they show both substantial amounts of Pb loss and radiogenic Pb. The Pb loss is also substantiated by the negative correlation between U concentrations and $^{206}Pb/^{238}U$ ages, which is most evident in the zircons of samples 674 and 677 (Fig. S1). The zircon grains from three samples define mean $^{206}Pb/^{238}U$ ages of 320.1 ± 3.7 Ma (2σ, $n = 24$, sample 657), 325.6 ± 3.3 Ma (2σ, $n = 18$, sample 674) and 323.2 ± 3.8 Ma (2σ, $n = 23$, sample 677) (Fig. S1). These mean $^{206}Pb/^{238}U$ ages are indistinguishable from the corcordia ages within the analytical uncertainty.

To sum up, the zircon grains from all the dated samples underwent variable degrees of Pb loss. Both single zircon evaporation and LA-ICP-MS U–Pb zircon ages, 326–322 Ma, consistently suggest that the dikes of leucogranite are coeval with that of the host mafic-ultramafic rocks, and the emplacement of the mafic-ultramafic cumulate rocks occurred at the Early to Late Carboniferous boundary.

9. Trace element compositions of minerals

Trace element compositions of clinopyroxene, orthopyroxene, plagioclase and olivine were analyzed from an ilmenite-bearing gabbronorite sample (type-II, 421), clinopyroxene from a plagioclase-amphibole wehrlite (537B) and hornblende compositions from an anorthosite (2A) by laser ablation inductively coupled plasma mass spectrometry.

Olivine and orthopyroxene contain low concentrations of incompatible elements including rare earth elements (Fig. 13a; Table S12). On the other hand, clinopyroxene and amphibole contain high concentrations of incompatible elements. Plagioclase is characterized by a high abundance of light REE. Plagioclase displays REE concentrations decreasing from light to heavy REE and a marked positive Eu anomaly. Orthopyroxene is characterized by low REE concentrations, steadily increasing from light to heavy REE. Due to analytical uncertainty (poor counting statistics), heavy REE in plagioclase, light and middle REE in olivine and orthopyroxene are poorly constrained. The REE pattern of clinopyroxene is characterized by marked enrichment of middle REE relative to light and heavy REE. Clinopyroxene from the plagioclase-amphibole wehrlite displays compositional zoning whereby the rims have slightly higher concentrations of light REE and marked negative Eu anomaly with respect to the cores. Clinopyroxenes from the ilmenite-bearing gabbronorite have 2.5 to 3.0 times higher REE concentrations than those in the plagioclase-amphibole wehrlite, and a more marked Eu anomaly (Fig. 13a), but lower abundances of Ba, Th, U, Pb and Cr. On the multi-element variation diagrams, the clinopyroxenes from the plagioclase-amphibole wehrlite display negative anomalies of Ba, Nb, Ta, Sr, P, Zr, Hf and Ti anomalies (Fig. 13b). Chondrite-normalized REE patterns of hornblende are similar to those of clinopyroxene (convex-downward, spoon-shaped), whereby REE abundances are roughly three times higher than clinopyroxene.

10. Discussion

10.1. Depth of emplacement

The depth of emplacement can be constrained based on the combination of the pressure-temperature-time evolution of the metamorphic country rocks with the timing of the emplacement of the mafic-ultramafic intrusions. As pointed out above, the Pulur high-grade metamorphic rocks attained their thermal peak conditions of ≥820 °C and 0.8–0.7 GPa at 332–328 Ma, followed by a near-isothermal decompression to ~800–730 °C and 0.5–0.4 GPa (Topuz et al., 2004a). During the exhumation, the high-grade metamorphic rocks underwent extensive retrogression under greenschist- to subgreenschist-facies conditions (0.3–0.1 GPa and 410–230 °C) at 315–310 Ma (Topuz and Altherr, 2004). Given the timing of the emplacement of the mafic-ultramafic intrusions at 326–322 Ma, we deduce that the mafic-

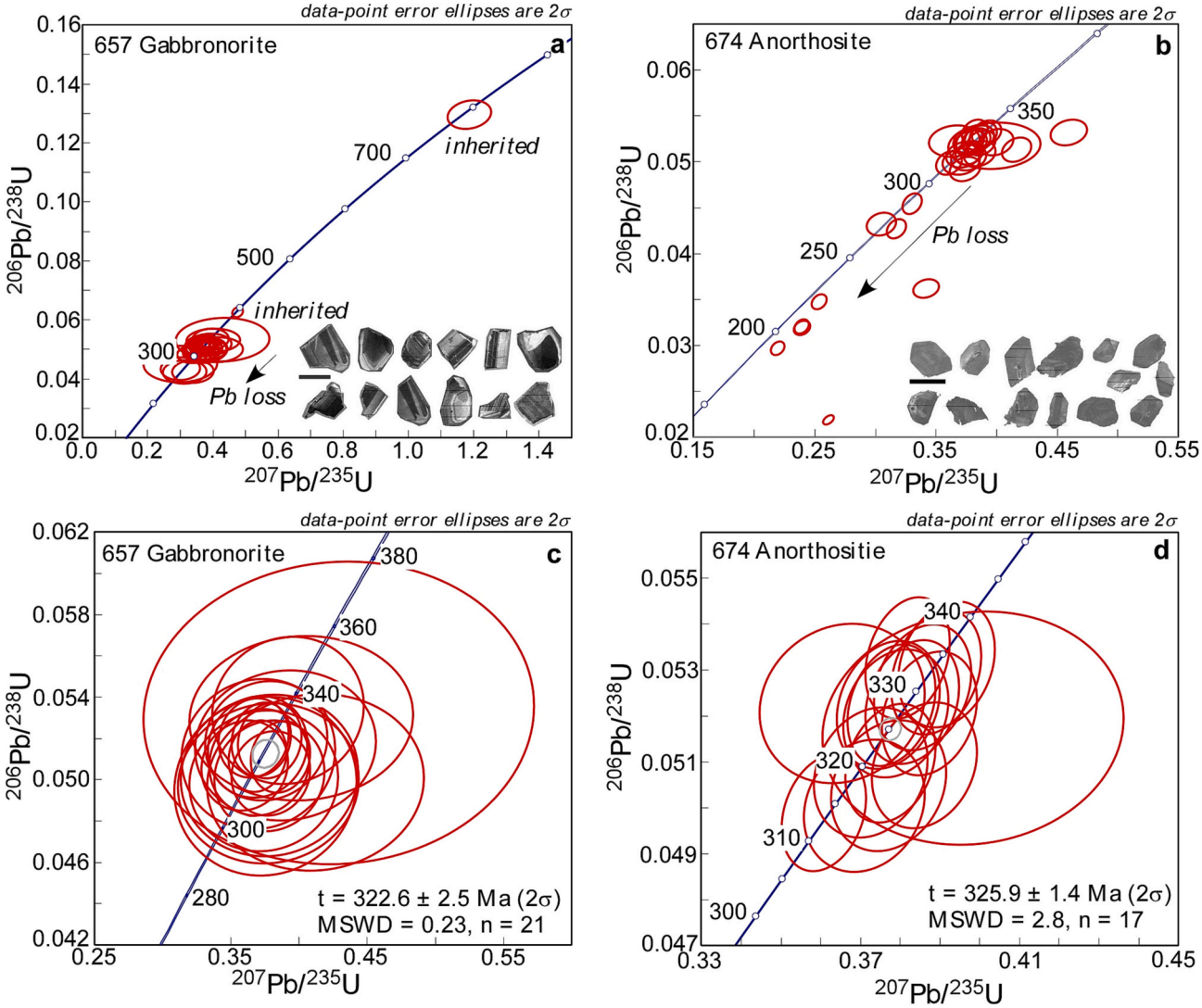

Fig. 12. Concordia diagrams of LA-ICP-MS U–Pb zircon ages from the gabbronorite (657) and the anorthosite (674). **a** and **b** show all analytical data together with CL images of the dated zircon grains, **c** and **d** only the analytical data used for age calculation.

ultramafic intrusions were emplaced after the near-isothermal decompression and before the subgreenschist- to greenschist-facies retrogression of the metamorphic country rocks. Thus, the metamorphic country rocks were probably at pressures of 0.5–0.3 GPa during the emplacement of the mafic-ultramafic intrusions.

The depth of emplacement of the intrusions can also be estimated by the two-pyroxene geothermobarometer. Compositions of coexisting clinopyroxene and orthopyroxene from both plagioclase-amphibole wehrlite and gabbronorite have been used to infer the equilibration temperature and pressure conditions after the model of Putirka (2008). As the geothermobarometer has been calibrated only for Mg-rich systems, only clinopyroxene compositions with $X_{Mg} > 0.76$ are used in the calculations. The calculations yielded temperatures and pressures of 930 ± 40 °C and 0.32 ± 0.06 GPa. The Fe–Mg partitioning coefficient between coexisting clinopyroxene and orthopyroxene pairs $(K_D(Fe-Mg)^{Cpx-Opx} = \left(\frac{X_{Fe}^{Cpx}}{X_{Mg}^{Cpx}}\right) \Big/ \left(\frac{X_{Fe}^{Opx}}{X_{Mg}^{Opx}}\right))$ is 0.69 ± 0.12, which is substantially lower than the putative igneous equilibrium value of 1.09 ± 0.14 and is characteristic for subsolidus conditions. These temperature and pressure values are interpreted to reflect those of the subsolidus conditions, and are consistent with the pressure constraints based on the temporal relationship between the metamorphic evolution of the metamorphic country rocks and the emplacement of the mafic-ultramafic intrusions (0.5–0.3 GPa, corresponding to crustal depths of 18–10 km).

10.2. Assimilation, fractionation and crystal accumulation

The presence of inherited zircon grains (only three grains among the dated 90 grains) suggests that some crustal material was assimilated during the crystallization of the basic magmas. Given the potentially high temperatures of basic magmas intruding into the middle continental crust, the assimilation of some crustal material is not unusual. The question here is whether the initial Sr-Nd-Pb isotopic signature resulted from the assimilation of crustal material. The initial isotopic ratios do not vary with rock type (Fig. 10). Hence, we regard it unlikely that the continental crust-like isotopic values are due to the assimilation of the crustal materials or mixing with the crustal melts. The plausible explanation is that the magmas of the mafic-ultramafic intrusions were derived from a subcontinental lithospheric mantle that was substantially metasomatized by sediment-derived fluids/melts. Overall, aqueous fluids liberated at the blueschist- to eclogite-facies transition are dilute, containing only moderate amounts of LILE, Sr and Pb, and do not transport significant amounts of LREE and Th (Hermann et al., 2006; Spandler et al., 2007; Turner and Langmuir, 2022; Yu et al., 2017). The

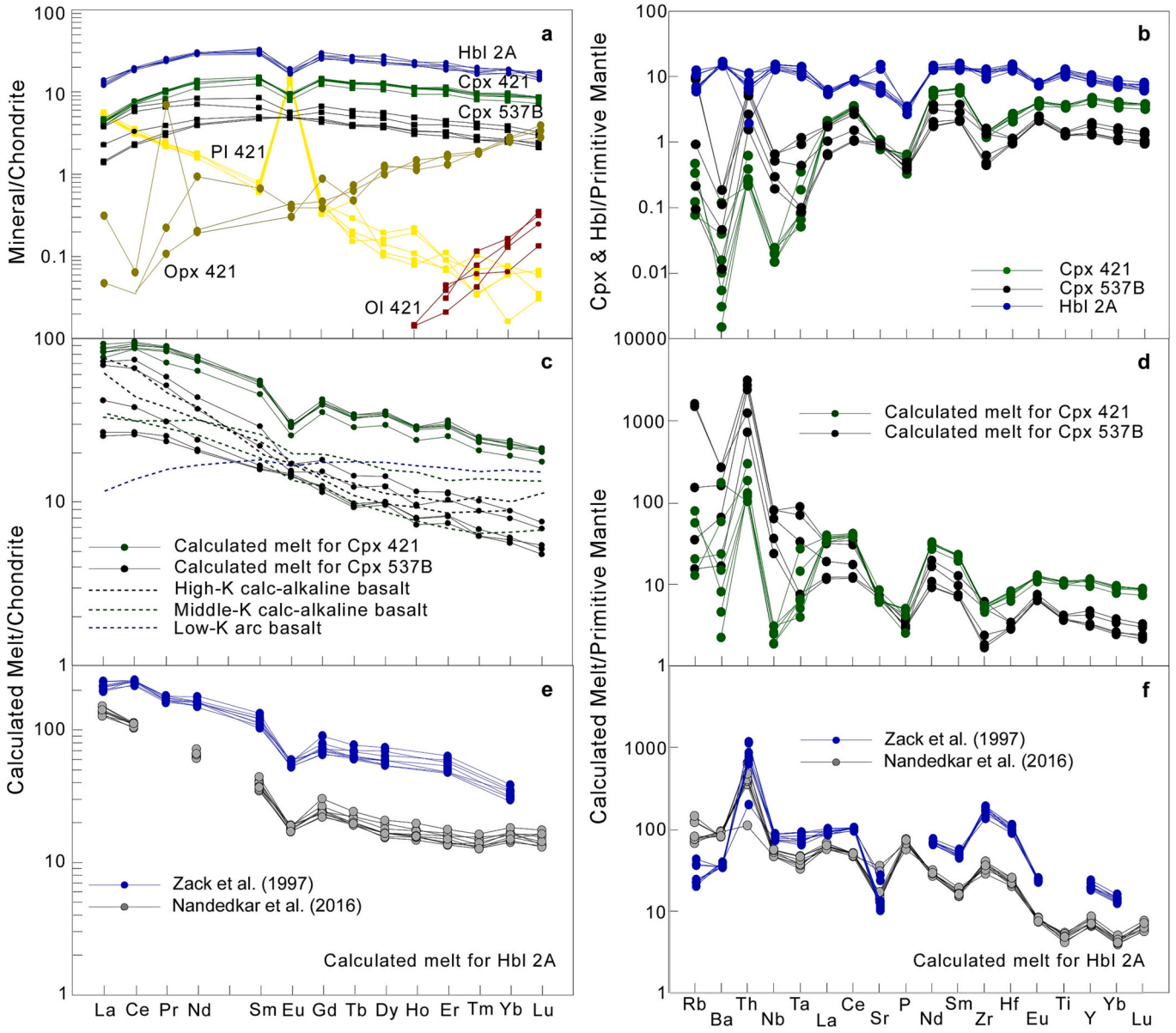

Fig. 13. **a** Rare earth element patterns of hornblende, clinopyroxene, orthopyroxene, plagioclase, and olivine. **b** Multi-element variation diagrams of clinopyroxene and hornblende. **c-d** REE patterns and multi-element variation diagrams of the calculated parental melts in equilibrium with clinopyroxene. For comparison, REE patterns of low-K tholeiite, middle- and high-K arc basalts are shown, taken from Fretzdorff et al. (2002), Gust et al. (1997) and Gertisser and Keller (2003). **e-f** REE patterns and multi-element variation diagrams of the calculated parental melts in equilibrium with hornblende.

budget of Th in subducting plate is dominated by sedimentary rocks. Th is insoluble in dehydration fluids and is only mobilized by melts. The calculated parental melts of the Pulur mafic-ultramafic rocks are characterized by marked positive Th anomalies on multi-element variation diagrams (Fig. 13d and f). Thus, the isotopic features possibly resulted from the substantial metasomatism of the lithospheric mantle by melts from metasedimentary rocks.

The cumulate rocks such as plagioclase-amphibole wehrlite, olivine gabbronorite and anorthosite possibly originated from a common magma by mineral fractionation and accumulation processes, suggested by the subparallel REE and multi-element variation patterns (Fig. 8). X_{Mg} values of the ferromagnesian minerals suggest that the plagioclase-amphibole wehrlite formed from more primitive melts, and gabbronorite and anorthosite from relatively fractionated melts (Table S7). On the other hand, X_{Mg} values of the ferromagnesian minerals and plagioclase composition in gabbronorite and anorthosite hardly differ from each other, implying that they are probably related to each other by accumulation processes rather than crystal fractionation.

The ilmenite-bearing gabbronorite, leucogranite and microdiorite did not originate by crystal fractionation from the same magma as the main cumulate body; this is inferred from the different shape of REE and multi-element variation patterns shown by these rocks (Fig. 9). The ilmenite-bearing gabbronorites were crystallized from variably fractionated magmas, as deduced by the wide compositional variation of olivine ($Fo_{79–45}$) and plagioclase ($An_{94–64}$). Type-I ilmenite-bearing gabbronorite is cumulate, while type-II (sample 535D) was probably derived from residual melts of type-I ilmenite-bearing gabbronorite (Fig. 9b). This interpretation is supported by the fact that the shape of the REE pattern of the calculated parental melts in equilibrium with clinopyroxene in sample 421 resembles that of type-II. The residual melt is characterized by a lower abundance of Al_2O_3 (ca. 14 wt%) and a higher abundance of CaO (19 wt%) with a CaO/Al_2O_3 ratio of 1.40 (Table S8). With these compositional features, it is diopside-hypersthene-olivine normative, and compositionally resembles ultra-

calcic melt inclusions and ankaramitic magmas in arcs (Kogiso and Hirschmann, 2001; Schiano et al., 2000; Médard et al., 2004).

All the cumulate rocks of the Pulur mafic-ultramafic intrusions show systematic positive Eu and Sr anomalies (Figs. 8 and 9a-b). Any complementary melt that is genetically related to the cumulate rocks should also show pronounced negative Eu and Sr anomalies. As the leucogranites and microdiorites are devoid of a consistent negative Eu anomaly, they cannot be related to the cumulate rocks by crystal fractionation. Partial melting studies on metabasalt yielded melts of dioritic composition at temperatures >1075–1100 °C and pressures of 0.8–1.5 GPa (e.g. Rapp and Watson, 1995). Such high temperatures are unlikely at the lower continental crust because they would lead to the large-scale melting of crustal lithologies. In addition, coeval igneous rocks which could be interpreted as unambiguous products of crustal melting are unknown in the region. Therefore, we regard it unlikely that the microdiorites represent the partial melting products of mafic underplates at lower crustal depths. Instead, the derivation from the fractionation of mantle-derived melts seems more probable. The leucogranites might represent either extreme fractionation products of the basic magmas in a deep crustal magma chamber or the direct partial melting products of underplated mafic rock. They cannot be regarded as fractionated melts of the microdiorites, since their emplacement postdates that of the leucogranites, and their multi-element variation diagrams do not resemble each other. The rare earth element and multi-element variation patterns of the leucogranites can be correlated with those of the Gümüşhane granite (Fig. 8c-d); the Gümüşhane granite shows a slightly high abundance of REE and a consistent negative Eu anomaly. Magmas of the Gümüşhane granite probably underwent plagioclase fractionation in a crustal magma chamber.

10.3. Parental magma compositions

Parental melt compositions of the Pulur mafic-ultramafic intrusions are constrained by minerals' major element compositions and the application of mineral/melt partition coefficients to trace element compositions of clinopyroxene and hornblende.

The co-existence of An-rich plagioclase ($An_{95–84}$) with moderately Fe-rich olivine ($Fo_{79–67}$) and the presence of large amphibole oikocrysts point to crystallization from hydrous magmas at middle to upper crustal depths (e.g., Beard, 1986; Panjasawatwong et al., 1997; Sisson and Grove, 1993). However, the water contents of the parental magmas of the Pulur mafic-ultramafic intrusions are difficult to quantify. Melekhova et al. (2015) refer the 0.6 wt% H_2O experiments as 'dry'; those with 2.3 wt% as 'damp' and those with 4.5 wt% as 'wet'. Overall, the experimental studies indicate that the crystallization sequence is dependent on the pressure, temperature and water content of parental magmas (Müntener et al., 2001; Blatter et al., 2013; Nandedkar et al., 2014; Melekhova et al., 2015). In all the Pulur mafic-ultramafic rocks, microtextural features clearly demonstrate that plagioclase crystallized earlier than amphibole. This sequence is observed in the experiments at damp conditions at pressures ≤0.5 GPa (Melekhova et al., 2015; Rezeau et al., 2021).

The sequence of the X_{Mg} values of the ferromagnesian minerals in the cumulate rocks is $X_{Mg}^{Cpx} > X_{Mg}^{Hbl} > X_{Mg}^{Opx} \geq X_{Mg}^{Ol}$. This sequence closely agrees with that predicted by mineral-melt Fe–Mg partition coefficients (Putirka, 2008, the references therein; $K_D^{\text{Fe-Mg}}{}_{\text{Ol-Melt}} = 0.31$, $K_D^{\text{Fe-Mg}}{}_{\text{Opx-Melt}} = 0.29$, $K_D^{\text{Fe-Mg}}{}_{\text{Hbl-Melt}} = 0.28$; $K_D^{\text{Fe-Mg}}{}_{\text{Cpx-Melt}} = 0.27$). However, the spread in X_{Mg} values in a single sample is large, varying between 0.05 and 0.12, which cannot represent the primary igneous equilibrium X_{Mg}. Consequently, Mg# numbers of equilibrium melt calculated for cumulus olivine ($Fo_{80–85}$) in amphibole-plagioclase wehrlite are significantly lower (Mg# 56–64) than those calculated for intercumulus clinopyroxene with X_{Mg} values of 0.85–0.92 in the same sample (Mg# 61–76). The large spread in the X_{Mg} values of the ferromagnesian minerals is comparable to that observed in the multilayer coronas between olivine and plagioclase in upper amphibolite- to granulite-facies metagabbros (e.g., Gallien et al., 2012; Joesten, 1986). Thus, the X_{Mg} values of the ferromagnesian minerals must haven largely controlled by the reaction with a melt phase and/or subsolidus diffusion. This interpretation is also supported by local resorbed outlines of cumulus minerals (Fig. 4a-d).

Relative to major divalent cation diffusion in ferromagnesian minerals, REE and trace element diffusions in silicate minerals are sluggish (Sun and Liang, 2017). Thus, REE and trace element composition of the parental melts of the mafic to ultramafic rocks can be calculated from the REE composition and the experimentally/empirically determined partition coefficients (Bédard, 2001; Jagoutz et al., 2007; Nandedkar et al., 2016; Tribuzio et al., 2008; Zack et al., 1997). As there are analytical uncertainties in measuring the trace elements in olivine (especially light and middle REE), plagioclase (especially heavy REE) and orthopyroxene (especially light REE) due to poor counting statistics and wide variations in the determined partition coefficients, we used trace element compositions of clinopyroxene and hornblende to constrain parental melt composition (Fig. 13c-f). Clinopyroxene/liquid partition coefficients were taken from Bédard (2001), and hornblende/liquid partition coefficients from Zack et al. (1997) and Nandedkar et al. (2016). Calcic amphibole/liquid partition coefficients vary considerably dependent on melt composition, pressure and melt structure. For the silica range 45–55 wt%, the partition coefficients for REE can change 2 to 3-fold. Overall, this involves uncertainty in the calculated melt composition, as partition coefficients also have a dependence on pressure and temperature.

The melt in equilibrium with intercumulus clinopyroxene from plagioclase-amphibole wehrlite (sample 537B) is characterized by moderately fractionated chondrite-normalized REE patterns ($(La/Yb)_{cn}$ = 4.5–6.8) (Fig. 13c). As the rim compositions are characterized by elevated LREE concentrations and slightly negative Eu anomalies relative to core compositions, diffusional effects are regarded as minimal. Although the calculated melt compositions in equilibrium with intercumulus clinopyroxene might not represent directly parental melt composition, none of the minerals crystallized earlier (Cr–Al spinel, olivine) apart from plagioclase are capable of fractionating light REE with respect to heavy REE. As the negative Eu anomaly is either absent to feeble, we can rule out significant plagioclase fractionation. Rare-earth element patterns of the calculated parental melt for the clinopyroxene composition in ilmenite-bearing gabbronorite are characterized by $(La/Yb)_{cn}$ ratio of 3.6–4.1 and pronounced negative Eu anomaly (Eu/Eu^* = 0.61–0.66), suggesting considerable plagioclase fractionation before clinopyroxene growth (Fig. 13c-d). Thus, the parental melt is expected to have had a much steeper REE pattern. The relatively fractionated nature of REE pattern is also verified by the calculated REE pattern of the parental melts in equilibrium with hornblende (La/Yb_{cn} = 5–8; Fig. 13e-f). It is noteworthy that the REE patterns calculated with the hornblende/liquid partition coefficients from Nandedkar et al. (2016) significantly deviate from those calculated with those from Zack et al. (1997). For comparison, REE patterns of low-K tholeiitic, middle- to high-K calc-alkaline basalts are also shown in Fig. 13c. The REE pattern of the calculated melt in equilibrium with intercumulus clinopyroxene from plagioclase-amphibole wehrlite and ilmenite-bearing gabbronorite resembles those of middle- to high-K calc-alkaline magmas and possibly mimics those of the parental magmas.

To summarize, the parental melts of the Pulur mafic-ultramafic cumulate rocks were characterized by enrichment of LILE relative to HFSE and light REE relative to heavy REE, as well as relative depletion of Nb, Ta and Ti, similar to the orogenic magmatic rocks (e.g. Gill, 1981; Tatsumi, 1989), and were probably middle- to high-K calc-alkaline basic melts.

10.4. Geodynamic setting and genesis of the coeval high-K calc-alkaline granites

Throughout the Sakarya Zone, Early Carboniferous was a time of L to M*P*-H*T* metamorphism (Okay and Topuz, 2017; Topuz et al., 2004a,

2007; Ustaömer et al., 2013). As pointed out above, the thermal peak of this metamorphism occurred during Visean (332–328 Ma). On the other hand, the ages of the large granite batholiths and age peaks of the detrital zircons from the Triassic accretionary complexes and Lower Jurassic sandstones in the Sakarya Zone define a period of high-volume magmatism at a time interval of 326–310 Ma (Ustaömer et al., 2016, Topuz et al., submitted); this high-volume magmatism postdates the peak of L to M*P*-H*T* metamorphism and occurred during the exhumation of metamorphic rocks. The Pulur mafic-ultramafic intrusions formed during the initial stages of this high-volume magmatism and could not have acted as a heat source for the L to M*P*-H*T* metamorphism in the region.

Geochemical and isotopic features of the mafic-ultramafic intrusions point to the presence of a lithospheric mantle that is significantly metasomatized by melts from the metasedimentary sources, possibly originating from continental subduction. Further evidence for the presence of an isotopically modified lithospheric mantle beneath the Sakarya Zone comes from predominantly negative values of εHf(i) values of the Carboniferous detrital zircons (348–310 Ma) from the Triassic accretionary complexes and Lower Jurassic sandstones (Topuz et al., submitted; Ustaömer et al., 2016). Timing of the accretion of the Sakarya Zone to the Laurussia is constrained as Early Carboniferous by the drastic change of age spectra of the detrital zircons in the sedimentary rocks of the Istanbul Zone, which is regarded as an eastern extension of Avalonia, and was already part of Laurussia during the Early Paleozoic (Akdoğan et al., 2021; Okay and Topuz, 2017). Thus, the mafic-ultramafic intrusions, the high-volume magmatism, formed in a post-collisional setting after the accretion of the Sakarya Zone to Laurussia (Fig. 14).

The Pulur L to M*P*-H*T* metamorphic rocks experienced isothermal decompression following the metamorphic peak, requiring that the continental crust was either thickened or of normal thickness during the metamorphic peak (e.g., Topuz et al., 2004a). For this reason, we set out from a thickened continental crust during the peak metamorphism (Fig. 14a). This continental crust was probably thinned before the high-volume magmatism. This interpretation is based on the fact that none of the Late Carboniferous magmatic rocks carry geochemical features compatible with the involvement of garnet in the source and during the magmatic fractionation. We tentatively suggest that convective thinning of the thickened lithospheric root might have triggered the voluminous magmatism in concert with crustal extension (Fig. 14b-c). High-K calc-alkaline I-type granitic rocks are commonly thought to have been derived from (i) fractional crystallization of middle to high-K basic melts, or (ii) partial melting of middle to high-K basic rocks at the lower crust (e.g., Roberts and Clemens, 1993; Sisson et al., 2005; Topuz et al., 2010). Several lines of evidence such as (i) the widespread presence of mafic microgranular enclaves in the granitic rocks, (ii) the absence/rarity of inherited zircons in the granitic rocks, (iii) identical Sr-Nd-Pb isotopic composition of the granitic rocks and the Pulur mafic-ultramafic rocks and (iv) middle- to high-K calc-alkaline nature of the parental melts of the Pulur cumulate rocks, suggest that the parental melts of the mafic-ultramafic rocks and those of coeval granites were genetically related. This genetic relationship is also supported by the similar/comparable geochemical characteristics of the leucogranitic dikes in the mafic-ultramafic complex (Fig. 8c-d). For this reason, we postulate that extension led to the formation of basic middle to high-K melts in the lithospheric mantle (Fig. 14c-d). These hydrous basic melts resulted in the formation of mafic underplates at the roots of the continental crust. Solidification of hydrous basic melts will exsolve aqueous fluids, which might lead to water-fluxed melting in overlying crustal lithologies and the formerly underplated mafic rocks. Water-fluxed melting of the mafic underplates by new basic magma injections can give rise to the formation of the high-K calc-alkaline I-type granitic rocks, as suggested by Collins et al. (2016) for the Cordilleran batholiths. Parts of the mafic melts with lesser water contents than the underplated ones were emplaced at middle crustal depths. Fractional crystallization in conjunction with mineral accumulation processes produced mafic-ultramafic cumulate rocks, described here.

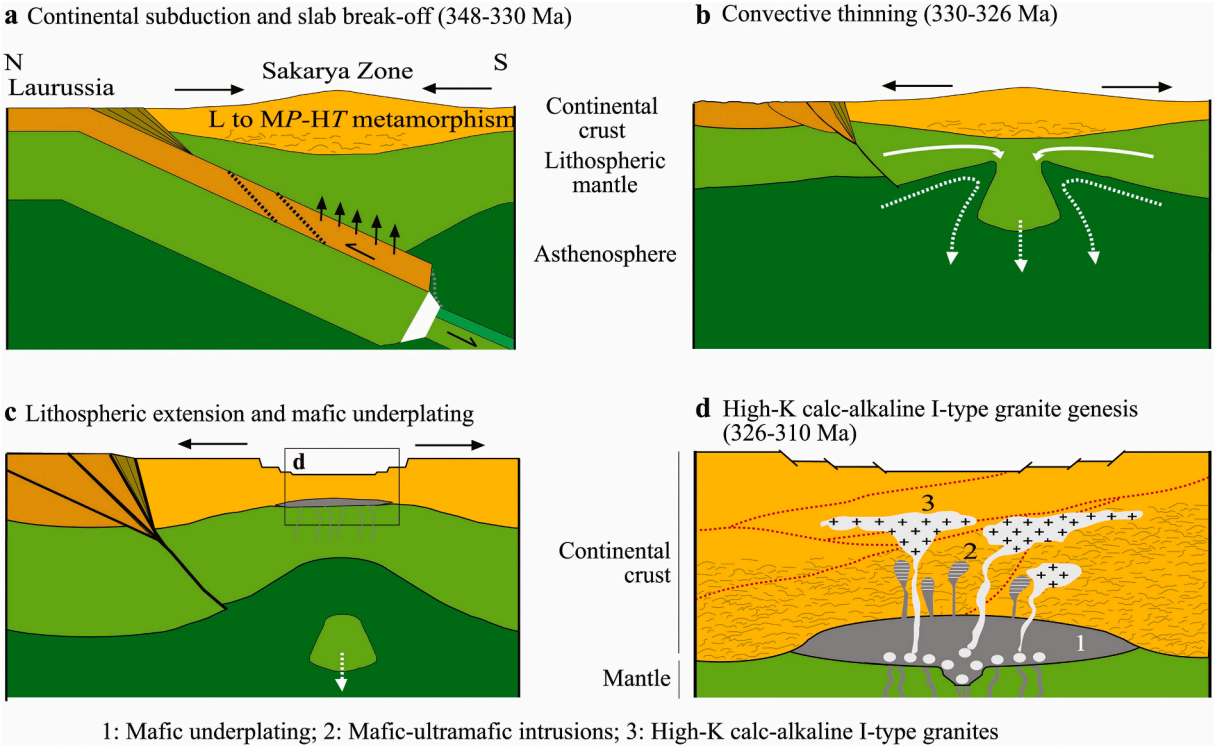

Fig. 14. A geodynamic model for the genesis of the mafic-ultramafic cumulate rocks and coeval high-K calc-alkaline I-type granites in the Eastern Pontides.

10.5. Comparison with the Alaskan-type ultramafic-mafic intrusive complexes

Both the regional geological framework and the geochemical features suggest that the Pulur mafic to ultramafic intrusions formed in an orogenic setting. Bektaş and Güven (1996) and Eyüboğlu et al. (2010) interpreted the Pulur mafic-ultramafic intrusions as the Alaskan-type ultramafic-mafic intrusive complexes. The Alaskan-type ultramafic-mafic intrusive complexes are regarded as a special category of orogenic ultramafic-mafic intrusions (e.g., Batanova et al., 2005; Himmelberg and Loney, 1995; Spandler et al., 2003; Thakurta, 2018), and are characterized by (i) funnel-shaped cross-sections, (ii) concentric zonation with central dunite grading outward into wehrlite, olivine clinopyroxenite, hornblende clinopyroxenite and hornblendite, which is ascribed to successive crystal-mush injections from deep-seated magma chambers, (iii) mineral assemblages involving olivine, clinopyroxene, magnetite and hornblende, and mostly devoid of orthopyroxene and plagioclase, and (iv) local occurrence of titanium-vanadium magnetite and platinium-group element mineralizations. In clear distinction, the Pulur mafic-ultramafic intrusions do not show any obvious zonal structure, and do not contain any pyroxenite and hornblendite. Instead, anorthosite and gabbronorite are common constituents of the Pulur mafic-ultramafic intrusions. Hence, the interpretation of the Pulur mafic-ultramafic intrusions as Alaskan-type intrusive complexes is incorrect.

11. Conclusions

In the Pulur Complex (Eastern Pontides), the mafic-ultramafic intrusions were emplaced into high-*T* low-*P* granulite-facies metamorphic rocks at 326–322 Ma, ca. 8–5 Ma after the peak of the regional metamorphism and are synchronous with high-volume magmatism at 326–310 Ma. The intrusions are composed of dunite, plagioclase-amphibole wehrlite, gabbronorite, leucogabbronorite, anorthosite and ilmenite-bearing gabbronorite of cumulus origin, and crosscut by dikes of ilmenite-bearing gabbronorite, leucogranite and microdiorite. The parental magmas of the cumulate rocks were probably middle- to high-K calc-alkaline basic magmas, and those of the ilmenite-bearing gabbronorite hypersthene-normative Ca-rich melts also of middle- to high-K calc-alkaline affinity. The crosscutting dikes did not originate by crystal fractionation from the same magma as the main cumulate body. All the rock types are characterized by continental crust-like Sr-Nd-Pb isotopic signatures, which are ascribed to an origin from a lithospheric mantle metasomatized mainly by sediment-derived melts. Furthermore, these Sr-Nd-Pb isotopic characteristics are comparable to those of the coeval voluminous high-K calc-alkaline I-type granites in the region. We suggest that the high-K calc-alkaline I-type granites are produced by the melting of newly underplated middle- to high-K calc-alkaline basic rocks compositionally similar to the parental melts of the cumulate rocks. The high-volume magmatism was possibly associated with the removal of the lowermost parts of the thickened lithosphere in a post-collisional setting.

Supplementary data to this article can be found online at https://doi.org/10.1016/j.lithos.2022.106946.

Declaration of Competing Interest

The authors declare that they have no known competing financial interests or personal relationships that could have appeared to influence the work reported in this paper.

Acknowledgments

We thank Emilio Saccani and three anonymous reviewers for constructive reviews

that significantly helped to improve and clarify the manuscript, and the editor Di-Cheng Zhu for handling the manuscript. This study was financially supported by the Deutsche Forschungsgemeinschaft (DFG-Graduiertenkolleg no. 273 at Heidelberg) and by the Turkish Academy of Science (TÜBA-GEBIP program). Udo Geilenkirchen, Ilona Fin and Oliver Wienand are thanked for preparing high-quality thin sections. Our thanks also include İdris Akyüz and Süleyman Ölmez for their great hospitality and logistic support during fieldwork.

References

Akdoğan, R., Okay, A.I., Sunal, G., Tari, G., Meinhold, G., Kylander-Clark, A.R., 2017. Provenance of a large lower cretaceous turbidite submarine fan complex on the active Laurasian margin: central Pontides, northern Turkey. J. Asian Earth Sci. 134, 309–329.

Akdoğan, R., Hu, X., Okay, A.I., Topuz, G., Xue, W., 2021. Provenance of the Paleozoic to Mesozoic siliciclastic rocks of the Istanbul Zone constrains the timing of the Rheic Ocean closure in the Eastern Mediterranean region. Tectonics 40 e2021TC006824.

Batanova, V.G., Pertsev, A.N., Kamenetsky, V.S., Ariskin, A.A., Mochalov, A.G., Sobolev, A.V., 2005. Crustal evolution of island-arc ultramafic magma: galmoenan pyroxenite-dunite plutonic complex, Koryak Highland (Far East Russia). J. Petrol. 46, 1345–1356.

Beard, J.S., 1986. Characteristic mineralogy of arc-related cumulate gabbros: Implications for the tectonic setting of gabbroic plutons and for andesite genesis. Geology 14, 848–851.

Bédard, J.H., 2001. Parental magmas of the Nain Plutonic Suite anorthosites and mafic cumulates: a trace element modeling approach. Contrib. Mineral. Petrol. 141, 747–771.

Bektaş, O., Güven, I.H., 1996. Alaskan-appinitic type ultramafic and mafic complexes as the root zone of the Eastern Pontide magmatic arc (NE-Turkey). In: Proceedings Symposium Geology of the Black Sea Region, Ankara, pp. 189–196.

Blatter, D.L., Sisson, T.W., Hankins, W.B., 2013. Crystallization of oxidized, moderately hydrous arc basalt at mid-to lower-crustal pressures: implications for andesite genesis. Contrib. Mineral. Petrol. 166, 861–886.

Boynton, W.V., 1984. Cosmochemistry of the rare earth elements: Meteorite studies. In: Henderson, P. (Ed.), Rare Earth Element Geochemistry. Elsevier, Amsterdam, pp. 63–114.

Burns, L.E., 1985. The Border Ranges ultramafic and mafic complex, south-Central Alaska: cumulate fractionates of island-arc volcanics. Can. J. Earth Sci. 22, 1020–1038.

Collins, W.J., Huang, H.Q., Jiang, X., 2016. Water-fluxed crustal melting produces Cordilleran batholiths. Geology 44, 143–146.

DeBari, S.M., Coleman, R.G., 1989. Examination of the deep levels of an island arc: evidence from the Tonsina ultramafic-mafic assemblage, Tonsina, Alaska. J. Geophys. Res. 94, 4373–4391.

Dick, H.J.B., Bullen, T., 1984. Chromian spinel as a petrogenetic indicator in abyssal and alpine-type peridotites and spatially associated lavas. Contrib. Mineral. Petrol. 86, 54–76.

Dokuz, A., 2011. A slab detachment and delamination model for the generation of Carboniferous high-potassium I-type magmatism in the Eastern Pontides, NE Turkey: the Köse composite pluton. Gondwana Res. 19, 926–944.

Dokuz, A., Külekçi, E., Aydınçakır, E., Kandemir, R., Alçiçek, M.C., Pecha, M.E., Sünnetçi, K., 2017. Cordierite-bearing strongly peraluminous Cebre Rhyolite from the eastern Sakarya zone, NE Turkey: constraints on the Variscan orogeny. Lithos 278, 285–302.

Eyüboğlu, Y., Dilek, Y., Bozkurt, E., Bektaş, O., Rojay, B., Şen, C., 2010. Structure and geochemistry of an Alaskan-type ultramafic-mafic complex in the Eastern Pontides, NE Turkey. Gondwana Res. 18, 230–252.

Fretzdorff, S., Livermore, R.A., Devey, C.W., Leat, P.T., Stoffers, P., 2002. Petrogenesis of the back-arc east scotia ridge, South Atlantic Ocean. J. Petrol. 43, 1435–1467.

Gaetani, G.A., Grove, T.L., Bryan, W.B., 1993. The influence of water on the petrogenesis of subduction-related igneous rocks. Nature 365, 332–334.

Gallien, F., Mogessie, A., Hauzenberger, C.A., Bjerg, E., Delpino, S., Castro de Machuca, B., 2012. On the origin of multi-layer coronas between olivine and plagioclase at the gabbro–granulite transition, Valle Fértil–La Huerta Ranges, San Juan Province, Argentina. J. Metamorph. Geol. 30, 281–302.

Gertisser, R., Keller, J., 2003. Trace element and Sr, Nd, Pb and O isotope variations in medium-K and high-K volcanic rocks from Merapi Volcano, Central Java, Indonesia: evidence for the involvement of subducted sediments in Sunda Arc magma genesis. J. Petrol. 44, 457–489.

Gill, J.B., 1981. Orogenic Andesites and Plate Tectonics. Springer, Heidelberg, p. 390.

Gust, D.A., Arculus, R.J., Kersting, A.B., 1997. Aspects of magma sources and processes in the Honshu arc. Can. Mineral. 35, 347–365.

Hart, S.R., 1984. A large-scale isotope anomaly in the southern hemisphere mantle. Nature 309, 753–757.

Hastie, A.R., Kerr, A.C., Pearce, J.A., Mitchell, S.F., 2007. Classification of altered volcanic island arc rocks using immobile trace elements: development of the Th–Co discrimination diagram. J. Petrol. 48, 2341–2357.

Hawthorne, F.C., Oberti, R., 2007. Classification of the amphiboles. In: Hawthorne, F.C., Oberti, R., Ventura, G.D., Mottana, A. (Eds.), Amphiboles: Crystal Chemistry, Occurrence and Health Issues: Rev. Mineral. Geochem., vol. 67, pp. 55–88.

Hermann, J., Spandler, C., Hack, A., Korsakov, A.V., 2006. Aqueous fluids and hydrous melts in high-pressure and ultra-high pressure rocks: implications for element transfer in subduction zones. Lithos 92, 399–417.

Himmelberg, G.R., Loney, R.A., 1995. Characteristics and petrogenesis of ultramafic-mafic intrusions, southeastern Alaska. In: U.S. Geological Survey Professional Paper, 1564, 47 p.

Holness, M.B., 2021. Cumulates and layered igneous rocks. In: Encyclopedia of Geology, 2nd edition, pp. 99–112. https://doi.org/10.1016/B970-12-409548-9.12460-1.

Jagoutz, O., Müntener, O., Ulmer, P., Pettke, T., Burg, J.P., Dawood, H., Hussain, S., 2007. Petrology and mineral chemistry of lower crustal intrusions: the Chilas complex, Kohistan (NW Pakistan). J. Petrol. 48, 1895–1953.

Jan, M.Q., Windley, B.F., 1990. Chromian spinel-silicate chemistry in ultramafic rocks of the Jijal complex, Northwest Pakistan. J. Petrol. 31, 667–715.

Joesten, R., 1986. The role of magmatic reaction, diffusion and annealing in the evolution of coronitic microstructure in troctolitic gabbro from Risör, Norway. Mineral. Mag. 50, 441–467.

Karslı, O., Dokuz, A., Kandemir, R., 2016. Subduction-related Late Carboniferous to Early Permian Magmatism in the Eastern Pontides, the Camlik and Casurluk plutons: insights from geochemistry, whole-rock Sr–Nd and in situ zircon Lu–Hf isotopes, and U–Pb geochronology. Lithos 266, 98–114.

Kaygusuz, A., Arslan, M., Siebel, W., Sipahi, F., İlbeyli, N., 2012. Geochronological evidence and tectonic significance of Carboniferous magmatism in the Southwest Trabzon area, eastern Pontides, Turkey. Int. Geol. Rev. 54, 1776–1800.

Kaygusuz, A., Arslan, M., Sipahi, F., Temizel, İ., 2016. U–Pb zircon chronology and petrogenesis of Carboniferous plutons in the northern part of the Eastern Pontides, NE Turkey: constraints for Paleozoic magmatism and geodynamic evolution. Gondwana Res. 39, 327–346.

Kogiso, T., Hirschmann, M.M., 2001. Experimental study of clinopyroxenite partial melting and the origin of ultra-calcic melt inclusions. Contrib. Mineral. Petrol. 142, 347–360.

Liew, T.C., Hofmann, A.W., 1988. Precambrian crustal components, plutonic associations, plate environment of the Hercynian Fold Belt of Central Europe: indications from a Nd and Sr isotopic study. Contrib. Mineral. Petrol. 98, 129–138.

Liu, Z., Zhu, D.C., Wang, Q., Eyuboglu, Y., Zhao, Z.D., Liu, S.A., Xu, L.J., 2018. Transition from low-K to high-K calc-alkaline magmatism at approximately 84 Ma in the Eastern Pontides (NE Turkey): magmatic response to slab rollback of the Black Sea. J. Geophys. Res. Solid Earth 123, 7604–7628.

Médard, E., Schmidt, M.W., Schiano, P., 2004. Liquidus surfaces of ultracalcic primitive melts: formation conditions and sources. Contrib. Mineral. Petrol. 148, 201–215.

Melekhova, E., Blundy, J., Robertson, R., Humphreys, M.C., 2015. Experimental evidence for polybaric differentiation of primitive arc basalt beneath St. Vincent, Lesser Antilles. J. Petrol. 56, 161–192.

MTA, 2002. 1:500.000 Geological Map of Turkey, Trabzon Sheet. Maden Tetkik ve Arama Genel Müdürlügü, Ankara.

Müntener, O., Kelemen, P.B., Grove, T.L., 2001. The role of H_2O during crystallization of primitive arc magmas under uppermost mantle conditions and genesis of igneous pyroxenites: an experimental study. Contrib. Mineral. Petrol. 141, 643–658.

Nandedkar, R.H., Hürlimann, N., Ulmer, P., Müntener, O., 2016. Amphibole–melt trace element partitioning of fractionating calc-alkaline magmas in the lower crust: an experimental study. Contrib. Mineral. Petrol. 171, 71.

Nandedkar, R.H., Ulmer, P., Müntener, O., 2014. Fractional crystallization of primitive, hydrous arc magmas: an experimental study at 0.7 GPa. Contrib. Mineral. Petrol. 167, 1015 https://doi.org/10.1007/s00410-014-1015-5.

Nzegge, O.M., Satır, M., Siebel, W., Taubald, H., 2006. Geochemical and isotopic constraints on the genesis of the late Paleozoic Deliktaş and Sivrikaya granites from the Kastamonu granitoid belt (Central Pontides, Turkey). Neues Jb. Mineral. Abh. 183, 27–40.

Okay, A.I., Göncüoğlu, M.C., 2004. Karakaya complex: a review of data and concepts. Turk. J. Earth Sci. 13, 77–95.

Okay, A.I., Leven, E.-J., 1996. Stratigraphy and paleontology of the upper Paleozoic sequences in the Pulur (Bayburt) region, Eastern Pontides. Turk. J. Earth Sci. 5, 145–155.

Okay, A.I., Topuz, G., 2017. Variscan orogeny in the Black Sea region. Int. J. Earth Sci. 106, 569–592.

Okay, A.I., Satır, M., Siebel, W., 2006. Pre-Alpide orogenic events in the Eastern Mediterranean region. In: Gee, D.G., Stephenson, R.A. (Eds.), European Lithosphere Dynamics, Geological Society of London Memoirs, vol. 32, pp. 389–405.

Okay, A.I., Sunal, G., Sherlock, S., Kylander-Clark, A.R., Özcan, E., 2020. İzmir-Ankara Suture as a Triassic to cretaceous plate boundary—Data from Central Anatolia. Tectonics 39 e2019TC005849.

Panjasawatwong, Y., Danyushevsky, L.V., Crawford, A.J., Harris, K.L., 1997. An experimental study of the effects of melt composition on plagioclase-melt equilibria at 5 and 10 kbars: implications for the origin of magmatic high-an plagioclase. Contrib. Mineral. Petrol. 118, 420–432.

Poller, U., Huth, J., Hoppe, P., Williams, I.S., 2001. REE, U, Th, and Hf distribution in zircon from western Carpathian Variscan granitoids: a combined cathodoluminescence and ion microprobe study. Am. J. Sci. 301, 858–876.

Putirka, K.D., 2008. Thermometers and barometers for volcanic systems. Rev. Mineral. Geochem. 69, 61–120.

Rapp, R.P., Watson, E.B., 1995. Dehydration melting of metabasalt at 8–32 kbar: implications for continental growth and crust-mantle recycling. J. Petrol. 36, 891–931.

Rezeau, H., Klein, B.Z., Jagoutz, O., 2021. Mixing dry and wet magmas in the lower crust of a continental arc: new petrological insights from the Bear Valley Intrusive Suite, southern Sierra Nevada, California. Contrib. Mineral. Petrol. 176, 1–25.

Roberts, M.P., Clemens, J.D., 1993. Origin of high-potassium, calc-alkaline, I-type granitoids. Geology 21, 825–828.

Rollinson, H., 2008. The geochemistry of mantle chromitites from the northern part of the Oman ophiolite: inferred parental melt compositions. Contrib. Mineral. Petrol. 156, 273–288.

Ross, P.S., Bédard, J.H., 2009. Magmatic affinity of modern and ancient subalkaline volcanic rocks determined from trace-element discriminant diagrams. Can. J. Earth Sci. 46, 823–839.

Saccani, E., Tassinari, R., 2015. The role of MORB and SSZ magma-types in the formation of Jurassic ultramafic cumulates in the Mirdita ophiolites (Albania) as deduced from chromian spinel and olivine chemistry. Ofioliti 40, 37–56.

Schiano, P., Eiler, J.M., Hutcheon, I.D., Stolper, E.M., 2000. Primitive CaO-rich, silica-undersaturated melts in island arcs: evidence for the involvement of clinopyroxene-rich lithologies in the petrogenesis of arc magmas. Geochem. Geophys. Geosyst. 1 (5).

Sisson, T.W., Grove, T.L., 1993. Experimental investigations of the role of H_2O in calc-alkaline differentiation and subduction zone magmatism. Contrib. Mineral. Petrol. 113, 143–166.

Sisson, T.W., Ratajeski, K., Hankins, W.B., Glazner, A.F., 2005. Voluminous granitic magmas from common basaltic sources. Contrib. Mineral. Petrol. 148, 635–661.

Spandler, C.J., Arculus, R.J., Eggins, S.M., Mavrogenes, J.A., Price, R.C., Reay, A.J., 2003. Petrogenesis of the Greenhills Complex, Southland, New Zealand: magmatic differentiation and cumulate formation at the roots of a Permian island-arc volcano. Contrib. Mineral. Petrol. 144, 703–721.

Spandler, C., Mavrogenes, J., Hermann, J., 2007. Experimental constraints on element mobility from subducted sediments using high-P synthetic fluid/melt inclusions. Chem. Geol. 239, 228–249.

Sun, C., Liang, Y., 2017. A REE-in-plagioclase–clinopyroxene thermometer for crustal rocks. Contrib. Mineral. Petrol. 172, 1–20.

Sun, S.-S., McDonough, W.F., 1989. Chemical and isotopic systematics of oceanic basalts: implications for mantle composition and processes. In: Saunders, A.D., Norry, M.J. (Eds.), Magmatism in the Oceanic Basins, vol. 42. Geological Society of London Special Publication, pp. 313–345.

Tatsumi, Y., 1989. Migration of fluid phase and genesis of basalt magmas in subduction zones. J. Geophys. Res. Solid Earth 94, 4697–4707.

Thakurta, J., 2018. Alaskan-type complexes and their associations with economic mineral deposits. In: Mondal, S.K., Griffin, W.L. (Eds.), Processes and Ore Deposits of Ultramafic-Mafic Magmas through Space and Time. Elsevier, pp. 269–302.

Topuz, G., Altherr, R., 2004. Pervasive rehydration of granulites during exhumation – an example from the Pulur complex, Eastern Pontides, Turkey. Mineral. Petrol. 81, 165–185.

Topuz, G., Altherr, R., Kalt, A., Satır, M., Werner, O., Schwarz, W.H., 2004a. Aluminous granulites from the Pulur complex, NE Turkey: a case of partial melting, efficient melt extraction and crystallization. Lithos 72, 183–207.

Topuz, G., Altherr, R., Satır, M., Schwarz, W.H., 2004b. Low-grade metamorphic rocks from the Pulur complex, NE Turkey: implications for the pre-Liassic evolution of the Eastern Pontides. Int. J. Earth Sci. 93, 72–91.

Topuz, G., Altherr, R., Schwarz, W.H., Dokuz, A., Meyer, H.-P., 2007. Variscan amphibolite-facies metamorphic rocks from the Kurtoğlu metamorphic complex (Gümüşhane area, Eastern Pontides, Turkey). Int. J. Earth Sci. 96, 861–873.

Topuz, G., Altherr, R., Siebel, W., Schwarz, W.H., Zack, T., Hasözbek, A., Barth, M., Satır, M., Şen, C., 2010. Carboniferous high-potassium I-type granitoid magmatism in the Eastern Pontides: the Gümüşhane pluton (NE Turkey). Lithos 116, 92–110.

Topuz, G., Göçmengil, G., Rolland, Y., Çelik, Ö.F., Zack, T., Schmitt, A.K., 2013. Jurassic accretionary complex and ophiolite from Northeast Turkey: no evidence for the Cimmerian continental ribbon. Geology 45, 255–258.

Topuz, G., Okay, A.I., Altherr, R., Schwarz, W.H., Sunal, G., Altınkaynak, L., 2014. Triassic warm subduction in Northeast Turkey: evidence from the Ağvanis metamorphic rocks. Island Arc 23, 181–205.

Tribuzio, R., Tiepolo, M., Fiameni, S., 2008. A mafic-ultramafic cumulate sequence derived from boninite-type melts (Niagara Icefalls, northern Victoria Land, Antarctica). Contrib. Mineral. Petrol. 155, 619–633.

Turner, S.J., Langmuir, C.H., 2022. Sediment and ocean crust both melt at subduction zones. Earth Planet. Sci. Lett. 584, 117424.

Ustaömer, P.A., Ustaömer, T., Robertson, A.H.F., 2012. Ion probe U-Pb dating of the Central Sakarya Basement: a peri-Gondwana terrane intruded by late lower Carboniferous subduction/collision-related granitic rocks. Turk. J. Earth Sci. 21, 905–932.

Ustaömer, T., Robertson, A.H.F., Ustaömer, P.A., Gerdes, A., Peytcheva, I., 2013. Constraints on Variscan and Cimmerian magmatism and metamorphism in the Pontides (Yusufeli–Artvin area), NE Turkey from U–Pb dating and granite geochemistry. In: Robertson, A.H.F., Parlak, O., Ünlügenç¸ U.C. (Eds.), Geological Development of Anatolia and the Easternmost Mediterranean Region, vol. 372. Geological Society of London, Special Publications, pp. 49–74.

Ustaömer, T., Ustaömer, P.A., Robertson, A.H., Gerdes, A., 2016. Implications of U–Pb and Lu–Hf isotopic analysis of detrital zircons for the depositional age, provenance and tectonic setting of the Permian–Triassic Palaeotethyan Karakaya Complex, NW Turkey. Int. J. Earth Sci. 105, 7–38.

Yu, Y., Sun, M., Huang, X.L., Zhao, G., Li, P., Long, X., Cai, K., Xia, X., 2017. Sr-Nd-Hf-Pb isotopic evidence for modification of the Devonian lithospheric mantle beneath the Chinese Altai. Lithos 284, 207–221.

Zack, T., Foley, S.F., Jenner, G.A., 1997. A consistent partition coefficient set for clinopyroxene, amphibole and garnet from laser ablation microprobe analysis of garnet pyroxenites from Kakanui, New Zealand. Neues Jahrbuch für Mineralogie, Abhandlungen 172, 23–41.